93-9028

Measurement of OH, H_2SO_4, MSA, NH_3 and DMSO Aboard the NASA P-3B Aircraft

NASA Grant No.: NCC-1-301
Georgia Tech Project No. G35-W92 (formerly A5716)

Final Report

June 1, 1998– May 31, 2001

Submitted to:

NASA Langley Research Center
Mail Stop 483
Hampton, VA 23681-0001

Attn: Richard Bendura

Submitted by:

School of Earth and Atmospheric Sciences
Georgia Institute of Technology
Atlanta, GA 30332

Principal Investigator: F. L. Eisele

Performance Report

This project involved the installation of a downsized multichannel mass spectrometer instrument on the NASA P-3B aircraft and its subsequent use on the PEM-Tropics B mission. The new instrument performed well, measuring a number of difficult-to-measure compounds and providing much new photochemical and sulfur data as well as possibly uncovering a new nighttime DMSO source. The details of this effort are discussed below.

The instrument used on PEM-Tropics B was the result of a previous downsizing project, and thus apart from some brief test flights the previous summer, it was participating in its first real mission. After the downsizer test flights several modifications were required prior to deployment on PEM-Tropics B. These were largely completed in the fall of 1998 and some additional laboratory testing was also accomplished in this same time frame. The new instrument was shipped to the Wallops Island Facility in very early January, and was installed shortly thereafter, delayed somewhat by the lack of an aircraft. The instrument initially had to be configured to operate from only 60 Hz power and later switched to a combination of 60 Hz and 400 Hz, as aircraft power became available. Installation went smoothly, but ground-based testing, particularly of the DMSO channel, was hampered somewhat by the large amount of hydrocarbon background in the closed-up hanger. Test flights just before departure yielded good results for the OH, H_2SO_4, and MSA measurement channel but some problems in the DMSO/NH_3 channel. The flight from Wallops to Dryden showed improvement of the DMSO channel, but still not proper functioning. There was little time on the transits from Dryden to Christmas Island for repairs, and while the OH, H_2SO_4, and MSA channel continued to function well, problems persisted or worsened in the DMSO/NH_3 channel.

The two inlets used to measure the above sets of compounds are very complex because of the sticky and/or reactive nature of the species. (For some of these compounds a simpler heated inlet might be used, except that such an inlet could evaporate the compound being measured from aerosols, thus causing a measurement

interference.) Therefore, a physically complex but nearly wall-less ambient temperature inlet is required. In an attempt to work on components inside of one of these complex inlets (DMSO) at Christmas Island, a bolt was broken off, which precluded future access to the internal components including the ion source at Christmas Island. It was not until additional tools could be brought to meet the aircraft at Tahiti that the bolt could be drilled out and the inlet removed. With the inlet off, loose fittings on the ion source were found and repaired. In hindsight, a greater effort should have been made to gain access to the ion source at Christmas Island, but at the time it was not clear that the critical problem was inside the inlet, and tools and time were very limited at Christmas. Once repaired, the DMSO channel provided much new and exciting data during the flights out of Tahiti and on the return portion of the mission. The OH, H_2SO_4, and MSA portion of the instrument continued to function well throughout the mission, with the exception of one or two brief periods when flights through very wet clouds caused shorting problems in the ion source. At the end of the mission, the P-3 returned to Wallops, our instrument was unloaded, and was shipped back to our laboratory for further calibration and testing of both the OH, H_2SO_4 and MSA and DMSO and HN_3 channels. The remainder of the first year was spent on data analysis. Overall, the new instrument performed well providing a great deal of new and interesting data.

The second year's effort on the project started just after the completion of the PEM-Tropics B mission. Data analysis continued in conjunction with more laboratory testing of the OH instrument. Improvements made to the down-sized OH instrument flown on PEM-Tropic B provided the first in situ calibrations of OH at high altitudes during daylight hours. In the past, in situ OH calibrations were done only below about 10,000 foot altitudes or at night when background OH was very low. The new high intensity dual output photolysis source used on PEM-Tropics B dramatically increased the number of calibrations made above 10,000 feet (because most flights take place during daylight hours when levels of ambient OH are as high or higher than those produced by the old calibration source at the low water concentration typically found above about 10,000 feet). These new calibrations lead to the surprising result that the OH instrument becomes more efficient and sensitive at higher altitudes. Initially not sure of this result, a laboratory study of several months duration was begun to verify and help

understand these findings. By the end of the study, it was concluded that the initially observed results were correct, and that the increased sensitivity for detecting OH was due to improved efficiency for sampling OH at lower pressures and temperatures. The decrease in pressure and temperature at high altitudes leads to a reduction in the Reynolds number in the ion source region, which reduces turbulence, wall loss, and mixing and results in a higher percentage of ambient OH reaching the measurement region. Flow prior to the calibration source is not affected by these parameters because the central axial flow does not come in contact with the walls and the actual flow velocity is measured. The final OH H_2SO_4 and MSA data were then submitted to the NASA data archive.

DMSO measurements were also conducted during PEM-Tropics B and resulted in some exciting new results. Most important among these is that DMSO appears to have an unexpected nighttime source. These measurements, however, also required many laboratory tests to insure their validity, since this was the first time that the ion chemistry scheme used to measure DMSO in PEM-Tropics B had been used on an aircraft. Calibration sources had to be retested and ground calibration had to be compared to in situ aircraft calibrations with isotopically labeled DMSO. The possible interference by several compounds had to be tested. The result of these tests suggests that the high observed DMSO is real, and no significant interferences could be found. The uncertainty in the data is, however, somewhat larger than anticipated due to problems with some commercially available permeation cell calibration sources of isotopically labeled DMSO. The DMSO data was then also submitted to the NASA data archive.

Ammonia measurements were less successful. While ammonia can easily be observed by our instrument its very sticky nature prevented a meaningful measurement. Even with very little exposed wall area in our sampling and ion source regions of the instrument ammonia was still lost to the walls and later re-emitted so that the measure ammonia signal had little relation to ambient ammonia concentrations.

The highlights of our PEM-Tropics B measurements were: an extensive mapping of the OH radical over the tropical Pacific Ocean, and the discovery that there must exist a nighttime source for DMSO (an important sulfur oxidation product).

The results of the present work were presented in a number of talks at the special spring 2000 AGU session in Washington, DC. A list of these talks is included as

Appendix A. This research effort also resulted in a number of manuscripts, which are listed in Appendix B. A more detailed discussion of the measurement techniques used and the scientific significance of the resulting measurements is included in the 4 papers included in Appendices C-F, which were written by our group.

Appendix A

Talks resulting from PEM-Tropics B

American Geophysical Union 2000 Spring Meeting, Washington, DC, May 30-June 3

1. Lee Mauldin, D. Tanner, C. Cantrell, E. Kosciuch, C. Gao, J. Nowak, D. Davis and F.L. Eisele. Hydroxyl radical measurements performed aboard the P-3 aircraft during PEM-Tropics B.
2. J. Nowak, D. Davis, G. Chen, F. Eisele, L. Mauldin, D. Tanner, C. Cantrell, E. Kosciuch, A. Bandy, D. Thornton, A. Clarke and V. Kapustin. A new source of marine sulfur?
3. R. Weber, B. Anderson, L. Thornhill, D. Tanner, R. Mauldin, E. Kosciuch, C. Cantrell, F. Eisele, A. Clarke, V. Kapustin and K. Moore. Comparison of atmospheric physical and chemical conditions under which large marine new particle formation events occur.
4. G. Grodzinsky, D. Davis, F. Eisele, L. Mauldin, D. Tanner, C. Cantrell, J. Crawford, S. Liu and Y. Wang. Latitudinal/altitudinal PEM-Tropics A/B OH distributions: Comparison of observations with models.
5. G. Chen, D. Davis, L. Wang, J. Crawford, D. O'Sullivan, B. Heikes, F. Eisele, R. Mauldin, D. Tanner, C. Cantrell, E. Kosciuch, B. Anderson, S. Liu, R. Shetter and B. Lefer. Boundary layer HO_x and O_3 chemistry based on PEM Tropics B airborne observations.
6. D. Davis, G. Chen, J. Nowak, F. Eisele, C. Cantrell, A. Clarke, V. Kapustin, R. Talbert, J. Dibb, A. Bandy and D. Thornton. A case study of the marine sulfur budget based on P-3 airborne observations recorded during PEM-Tropics B.

Appendix B

Papers Resulting from PEM-Tropics B

1. Nucleation in the equatorial Pacific during PEM Tropics B: Enhanced boundary layer H_2SO_4 but no particle production, R.J. Weber, K. Moore, V. Kapustin, A. Clarke, R.L. Mauldin, E. Kosciuch, C. Cantrell, F.Eisele, B. Anderson and L. Thornhill. Submitted to *Journal of Geophysical Research-Atmospheres.*
2. Marine latitude/altitude OH distributions: Comparison of Pacific Ocean observations with models, D. Davis, G. Grodzinsky, G. Chen, J. Crawford, F. Eisele, L. Mauldin, D. Tanner, C. Cantrell, W. Brune, D. Tan, I. Faloona, B. Ridley, S. Sandholm, G. Sachse, S. Vay, B. Anderson, M. Owens, B. Heikes, J. Snow, R. Shetter, B. Lefer, D. Blake, N. Blake, M. Carroll and Y. Wang, *Journal of Geophysical Research*, in press.
3. Chemical ionization mass spectrometry technique for the detection of dimethylsufoxide and ammonia, J.B. Nowak, L.G. Huey, F.L. Eisele, D.J. Tanner, R.L. Mauldin III, C. Cantrell, E. Kosciuch and D.D. Davis. Submitted to *Journal of Geophysical Research.*
4. Measurements of OH aboard the NASA P-3 during PEM-Tropics B, R.L. Mauldin III, F.L. Eisele, D.J. Tanner, C.A. Cantrell, E. Kosciuch, J.B. Nowak, G. Chen, L. Wang, D. Davis, B.A. Ridley and B. Lefer, *Journal of Geophysical Research*, in press.
5. The relationship between OH measurements on two different NASA aircraft during PEM-Tropics B, F.L. Eisele, R.L. Mauldin, D.J. Tanner, C. Cantrell, E. Kosciuch, J.B. Nowak, B. Brune, I. Faloona, D. Tan, D.D. Davis, L. Wang and G. Chen. *Journal of Geophysical Research*, in press.
6. Airborne observations of DMSO, DMS, and OH at marine tropical latitudes, J.B. Nowak, D.D. Davis, G. Chen, F.L. Eisele, R.L. Mauldin III, D.J. Tanner, C. Cantrell, E. Kosciuch, A. Bandy, D. Thornton and A. Clarke, *Geophysical Research Letters*, **28**, 2201-2204, 2001.

APPENDIX C

Measurements of OH aboard the NASA P-3 during PEM-Tropics B

R.L. Mauldin III, F.L. Eisele, D.J. Tanner, C.A. Cantrell, E. Kosciuch, J.B. Nowak, G. Chen, L. Wang, D. Davis, B.A. Ridley, and B. Lefer

Abstract.

Airborne measurements of the hydroxyl radical were performed aboard the NASA P-3B using the Selected Ion Chemical Ionization technique during the Pacific Exploratory Mission (PEM)-Tropics B study. Typical midday boundary layer OH concentrations of 6-7 x 10^6 molecule cm^{-3} were observed in the vicinity of Christmas Island (0-3°N), and 7-8 x 10^6 molecule cm^{-3} in the vicinity of Tahiti (17-22°S). Photochemical box model calculations of the concentration of OH ([OH]) throughout the entire mission yield generally good agreement (slope = 1.26) with a tendency for the model to slightly overestimate the measured OH. Boundary layer measurements of OH in an air mass containing low ozone concentrations (<5 ppbv) yielded a midday [OH] of ~5 x 10^6 molecule cm^{-3}, some 45% lower than 7 x 10^6 molecule cm^{-3} observed in air masses at the same latitude with more typical ozone concentrations (30-40 ppbv). Measurements performed under clouds yielded [OH] of ~2.5 x 10^6 molecule cm^{-3}, a value which is a factor of two lower when compared to data taken on either side of the cloud. This decrease corresponds to the decrease in $j(O_3)$ to produce $O(^1D)$.

1. Introduction

The hydroxyl radical (OH) is the principal oxidant in the Earth's lower atmosphere, reacting with a wide variety of compounds. While its concentration is typically less than a pptv (part per trillion by volume), its high reactivity makes it the primary tropospheric cleansing agent responsible for controlling the build-up of many compounds of both anthropogenic and biogenic origin. These compounds include such species as CO, CH_4, numerous other non-methane hydrocarbons and their oxidation products.

The primary source of tropospheric OH is the photolysis of ozone to produce $O(^1D)$ followed by the following reaction sequence:

$$O_3 + h\nu(< 330\ nm) \rightarrow O(^1D) + O_2(^1\Delta_g) \qquad j(O(^1D))$$

(R1) $$O(^1D) + H_2O \rightarrow 2OH$$

The photolysis of H_2O_2 and CH_3OOH can also produce OH directly but to a much smaller degree. Once formed, OH reacts primarily with CO and CH_4 in the remote troposphere to produce HO_2 and CH_3O_2 respectively, with the latter species eventually producing HO_2. The HO_2 (OH reservoir species) can react further to regenerate OH via the reactions:

(R2) $$HO_2 + NO \rightarrow OH + NO_2$$

(R3) $$HO_2 + O_3 \rightarrow OH + 2O_2$$

Thus the production of OH depends primarily on the available actinic flux (which determine the rates of photolysis), the $[O_3]$, and the $[H_2O]$; and secondarily upon the concentration of NO.

Recent measurements of OH in and around clouds reveal elevated OH concentrations. These enhanced levels of OH are attributed to increased levels of actinic

flux. Model calculations show that the clear sky actinic flux could be enhanced by as much as a factor of two [*Duynkerke and Van Weele*, 1991; *Madronich*, 1987]. While there has been work on the enhancement of OH concentrations above and inside clouds [*Mauldin et al.*, 1997, 1998, 1999], there has been little investigation of the depression of OH concentrations below clouds or the impact of clouds upon column OH concentrations.

In this work we present the results of airborne measurements of OH made aboard the NASA P-3B during PEM-Tropics B using the Selected Ion Chemical Ionization (SICIMS) technique. These results are compared to those calculated from a photochemical box model developed at the Georgia Institute of Technology. Other observations such as OH concentrations measured in the presence of low ozone concentrations, and above or beneath clouds are also discussed.

2. Experimental Technique

Measurements of OH were performed aboard the NASA P-3B using the SICIMS technique. A schematic diagram of the instrument used in this study can be found in Figure 1. The system consists of three major sections: a shrouded inlet which straightens and slows the air flow; an ion reaction region in which the chemical ionization reactions occur; and a turbo molecular pumped vacuum chamber which houses a quadrupole mass spectrometer and an electron multiplier detector. The measurement technique and system used in this study has been described in detail elsewhere [*Eisele and Tanner*, 1991; *Eisele and Tanner*, 1993, *Tanner et al.*, 1997; *Mauldin et al.*, 1998; *Mauldin et al.*, 1999]; therefore the reader is directed to those works for experimental details.

The method for determining the calibration coefficient, C, in equation (I) however bears some discussion as a different type of calibration assembly from that used in previous studies by our group was employed here. Briefly, the calibration technique involves producing a known amount of OH in front of the 1.9 cm curved sampling port by photolyzing ambient H_2O via the 184.9 nm emission line from a filtered Hg Pen-Ray Lamp. In the past, a band pass filter was used to separate the 184.9 nm emission line from the others present. This type of filtering works quite adequately at lower altitudes where H_2O concentrations are generally high. Problems arose however during the day at higher altitudes (>15,000 ft) where low H_2O concentrations allowed little OH to be produced from the calibration source when compared to ambient OH concentrations (except at night when few flights are flown). One solution to alleviate this situation would be to add a know quantity of H_2O into the sample air steam. This approach was deemed impractical due to the difficulties in adding large quantities of H_2O to large volumes of air in a known way. Another solution is to increase the light output of the calibration assembly. The bandpass filter passes 184.9 nm light with ~10% efficiency. If this efficiency could be increased while still maintaining the same level of rejection of the other emission lines, it would be possible to produce a larger known amount OH under low H_2O conditions.

A schematic diagram of the calibration assembly used in this study can be found in an insert in Figure 1. As can be seen, light passes from a temperature controlled Hg lamp through a quartz cylindrical lens (focal length = 2.54 cm). The light is then reflected off two mirrors mounted at 45° to the light path. These mirrors have been coated to selectively reflect 184.9 nm. Light exits the calibration housing through a Suprasil window and combination shutter/slit assembly, then passes through a 2.5 cm enclosed path

before illuminating the sample flow. The calibration housing is N_2 purged to prevent light absorption, and the build up of O_3 from the photolysis of O_2. Laboratory tests using this arrangement show an increase in the intensity of the 184.9 nm emission line in front of the curved inlet of a factor of 8 over the 184.9 nm bandpass filter used in previous studies. The shutter assembly has also been modified to allow for two photolysis settings (slit widths). The "narrow" setting (~1 mm) was approximately a factor of eight less intense as the "wide" setting (~8 mm) and mimicked the output of the calibration assembly used in the past. In practice it was found that at dew points greater than −10 °C, the "wide" setting produced such high concentrations of OH that the NO_3^- reagent ion began to be depleted significantly. Thus in general, low altitude calibrations used the "narrow" setting while the "wide" setting was used for high altitude determinations. As discussed later, calibrations performed under conditions where both slit settings produced reasonable concentrations of OH yielded good agreement between the two settings. One additional feature added to the inlet system for this study is a UV sensitive photodiode mounted on the inner 5.1 cm flow duct opposite the calibration light entrance (Figure 1). The output of this photodiode is not used in the calculation of the calibration factor but rather to monitor the output of the calibration assembly, permitting in flight checks of the exit window quality and output reproducibility as a function of altitude.

The OH concentration produced by the calibration source is a function of the intensity of the photon flux at 184.9 nm, the $[H_2O]$, the absorption cross-section at 184.9 nm, the yield of OH from H_2O photolysis, and the sample flow velocity. The flow velocity was measured using a Pitot tube mounted just forward of the 1.9 cm curved inlet, and the $[H_2O]$ was measured using a dew point hygrometer aboard the aircraft. The photon flux

at 184.9 nm was mapped out on the ground periodically during the study using a vacuum UV diode mounted on an x/y movable traverse. This vacuum UV diode was intercompared with a National Institute of Standards and Technology (NIST) standard diode prior to, and at the end of the mission. Recent measurements of the absorption cross-section of H_2O at 184.9 nm by *Creasy et al.* [2000], *Hofzumahaus et al.* [1997], and *Cantrell et al.* [1997] are in good agreement and yield values of 7.22×10^{-20}, 7.0×10^{-20}, 7.14×10^{-20} cm^2 $molecule^{-1}$ respectively. *Yoshino et al.* [1996] report a value of 1.02×10^{-19} cm^2 $molecule^{-1}$, however this value was obtained near the end of their detection limit. For this work, the value of 7.14×10^{-20} cm^2 $molecule^{-1}$ from *Cantrell et al.* [1997] was used as it is in good agreement with other measurements, and this value has been used for the reported values in earlier work [*Mauldin et al.*, 1998; *Mauldin et al.*, 1999]. It should be pointed out that all of these recent cross-section measurements are some 30-80% larger than the currently recommended value of 5.5×10^{-20} cm^2 $molecule^{-1}$ [*DeMore et al.*, 1997], a value based on the analysis by *Hudson* [1974] of measurements performed over 30 years ago.

Calibrations were performed periodically at various altitudes during each flight. The photon fluence was checked after every second or third flight. With the exception of one measurement, measurements of the lamp output were found to be constant to within 6% of each other for a given slit setting. The one measurement that fell outside of this range was not used and was caused by a dirty output window. This change was detected also by the monitoring diode. A calibration involved measuring the ambient OH concentration, then opening the shutter to a given slit setting allowing the photolysis of ambient H_2O. The calculated OH produced from the calibration source was then

compared to the signal rise observed after the shutter was opened. Figure 2 is a plot of the measured calibration coefficient as a function of ambient pressure. Each point is a single 30 s, measurement. The scatter in the points is thought to be due to the uncertainty in the H_2O concentration. This value is used twice in the calculation of the calibration coefficient. First it is used to calculate of the attenuation of the lamp output reaching the sampling inlet. Second it is used directly in the photolysis equation used to calculate the [OH] produced. The dew point hygrometer aboard the aircraft had a response time on the order of 10's of seconds. While not desirable, as a matter of practicality the dew point was found to change during some calibrations producing the observed scatter.

The plot the points are grouped into two categories, high altitude lens setting and low altitude lens setting each with narrow and wide slit values. As can be seen at altitudes where both narrow and wide slit settings were used, the calculated calibration values are indistinguishable. During the flights it was found that the voltages on outside atmospheric pressure electrostatic lenses needed to be adjusted to maintain high signal levels as the ambient pressure changed with changing altitude. Typically these voltages only changed between two different settings, one for high altitudes and one for low. While controlling the observed signal level, these settings also determine the lifetime in the ion reaction region. Thus, as a consequence of changing these settings, the efficiency that $H^{34}SO_4^-$ (and HSO_4^-) ions are formed is also changed. This fact is revealed in the calibration values measured at 700 mb shown in Figure 2. The average of the high altitude lens values is 6.00×10^9 while the average of the low altitude settings is 7.75×10^9 molecule cm^{-3}, indicating that the high altitude settings are more efficient at producing $H^{34}SO_4^-$ ions. A linear fit to calibrations taken at either lens setting is also shown in Figure 2. Depending

upon the lens values recorded during the measurement, either the fit to the high or low altitude data was used to obtain the OH concentrations presented here. Unfortunately, these lens voltages were not recorded at all times during the mission. OH concentrations measured during these periods were obtained either by using the average value of the calibration coefficient calculated for the two different lens settings for data taken at altitudes with pressures less than 850 mb or by using the low altitude lens fit for data taken at altitudes with pressures greater than or equal to 850 mb. The total reported error limits of ±40.0% are 2 sigma and correspond to the 95% confidence level referring to the total systematic and random errors for a given measurement. The uncertainty was obtained by a thorough propagation of error calculation. Data taken during periods where no lens voltages were recorded have an additional uncertainty of ±20% or a total uncertainty of ±60%. This increased uncertainty reflects the use of a "best guess" calibration value for that data.

It should be noted that high altitude OH concentrations presented in earlier work [*Mauldin et al.*, 1998; *Mauldin et al.*, 1999] were calculated using an exponential fit to calibration data. This fit began at a value of 9.8 at sea level, and rose to 14.8 at 465 mb. As stated earlier, it was difficult to perform calibrations at high altitudes during the daylight. As a result there was a large uncertainty in those calibration values obtained. In light of our present set of high altitude calibration values, the authors now feel that a lower calibration value should be used than was originally applied. A more appropriate value would be the line shown as Linear Fit A in *Mauldin et al.* [1998] and *Mauldin et al.* [1999]. Using this fit will not change the low altitude values, as the deviation from the exponential fit does not begin until ~10,000 ft. At 10,000 the correction is <4%, rising to

a maximum correction at altitudes greater than or equal to 18,000 of ~38%. While this change is significant, it applies only to data taken at higher altitudes and not to boundary or buffer layer measurements where most of these studies were conducted.

The results presented here are given as 30 s measurements. A typical 30 s measurement consisted of an 8 sec measurement of mass 99 ($H^{34}SO_4^-$), with only $^{34}SO_2$ and N_2 being added through the front set of injectors in the curved sampling port. At the end of this 8 s measurement (called the OH signal measurement), the flow of N_2 is replaced by propane to remove any OH present. While waiting for this flow to equilibrate, mass 62 (NO_3^-), mass 97 (HSO_4^-), and an electronic background were measured for 1, 4, and 2 s respectively. Next mass 99 was measured again for 8 s (called the OH background measurement). At the end of this OH background measurement, the propane flow is turned off and N_2 again added. While waiting on this flow to equilibrate, mass 62 (NO_3^-), mass 97 (HSO_4^-), and mass 95 (MS^-) were measured for 1, 4, and 2 s respectively. The value of HSO_4^- in equation (I) above is the time normalized counts at mass 99 without propane present in the front injector minus the time normalized counts with propane flowing. In this manner we report [OH], [H_2SO_4], and [MSA] once every 30 s, although it is possible to report [H_2SO_4] once every 15 s.

3. Measurements and Modeling Results

The results of OH measurements performed during the entire PEM-Tropics B campaign are shown in Figure 3. The data are presented as 30 s measurements using the technique described above. The gaps present in the data are due to several different reasons. The data shown have been filtered to remove any points deemed to have

unacceptable auxiliary parameters, including flows, lens settings, electrical noise, or background signal. Data taken during times of calibrations have also been removed, as the concentrations of OH produced are so large that it is not possible to reliably retrieve ambient OH concentrations during these periods. The remaining gaps are times where OH was not measured to gain better precision on other species being measured by the instrument such as 1 Hz H_2SO_4 data for nucleation studies, or periods where the instrument was taken off line due to dense precipitation or to perform diagnostics or repair work. For reference purposes, an altitude profile is also presented for each flight. As can be seen, most of the large-scale structure or variability is due to changes in altitude. The smaller scale features observed in many of the flights are due to changes in [H_2O], j(O_3) and/or changes in [NO]. It should be noted that the OH high frequency scatter actually decreases percentage wise with increasing [OH]. As this is a fast OH measurement technique, it is possible to capture "fast" changes due to changes in [H_2O]. While there were fast O_3 and NO, there was no fast H_2O measurement aboard the P3-B.

The period of 04:00 to 05:00 UTC during flight 14 was flown in the dark and is a good example of the precision that the instrument is capable of when measuring low [OH]. Typical 5 min averages during this time period yield values of (3-5 $\pm$ 10) x 10^4 molecule cm^{-3}. Under clear cloudless conditions, the average midday boundary layer concentration of OH was ~6-7 x 10^6 molecule cm^{-3} in the vicinity of Christmas Island (0-3°N) and 7-8 x 10^6 molecule cm^{-3} in the vicinity of Tahiti (17-22°S).

Photochemical box model simulations of the data shown in Figure 3 were performed using a model developed at the Georgia Institute of Technology (Ga. Tech.). The model used for these simulations is described fully elsewhere here [*Wang et al.*, this

issue]; thus only relevant details will be discussed. The model inputs were one-minute averages of the species measured aboard the aircraft that affect OH concentrations (O_3, $j(O_3)$, NO, CO, H_2O_2, hydrocarbons, etc). Reaction rates were based on the 1997 NASA JPL [*DeMore et al.*, 1997] and the 1997 J. Phys. Chem. Ref. Data [*Atkinson et al.*, 1997] recommendations.

An important new aspect to the model inputs is the values for photolysis rates or j values. In previous works involving OH modeling, it was necessary to use either corrected Eppley radiometer measurements or model calculations to determine photolysis rates [*McKeen et al.*, 1997; *Mauldin et al.*, 1997, 1998; *Davis et al.*, 1999 and references therein]. In this work however measured photolysis frequencies were used as model inputs. These values were obtained from two 2π str (combined to give 4π str total response) spectral radiometers mounted above and below the aircraft [*Lefer et al.*, this issue]. These photolysis rates should allow much better estimates of OH production, especially for regions in and around clouds.

A plot of measured vs modeled [OH] for flights 4-19 (the entire PEM-Tropics B campaign) is shown in Figure 4. Also shown is the 1:1 correlation line for reference. As can be seen with the exception of a few outlying points the agreement is generally good. A standard regression of this data yields a slope of 1.26 with a correlation coefficient of 0.93. This value of the slope indicates that the model has a slight general tendency to over-predict OH concentrations when compared to the measurements presented here. It should be pointed out however that this tendency is slight and that the agreement is well within the uncertainties of the measurements or model inputs.

P-3 Flight 14 was designed to investigate the HO_x chemistry at various altitudes from midday to sunset. The flight involved flying a wall profile with four altitudes, 1000, 4000, 10,000, and 18,000 ft. In flying a profile of this type, the each altitude can be sampled with the sun at different solar zenith angles. Figure 5 is a plot of the measured and modeled [OH] and is a good example of the typical agreement between the two. Also shown are $j(O_3)$ and $[H_2O]$, two parameters that directly control the production of OH, and an altitude profile. As can be seen the agreement between the measurement and model is generally quite good, despite the $[H_2O]$ and $j(O_3)$ changing by over a factor of 20 and 200 respectively throughout the flight. It is interesting to note that the largest discrepancy of ~60% occurs at 00:15 UTC at the highest altitude. However, at 01:45 UTC when the aircraft was again at 18,000 ft, the model and measurements show good agreement to the 18% level. Flight 10 also demonstrates the agreement between measurements and model under unusual conditions. During this flight low $[O_3]$ (<5 ppbv) were observed in the marine boundary layer. As $[O_3]$ also directly controls OH production, measurements and model should reflect the lower concentration. Figure 6 is a plot of measured and modeled OH together with observed $[O_3]$ and an altitude profile. As can be seen, the agreement is again quite good even with the $[O_3]$ changing by more than a factor of six as the aircraft changes altitude. The observed midday [OH] of ~5 x 10^6 molecule cm^{-3} is some 45% lower when compared with the value of 7 x 10^6 molecule cm^{-3} observed during flight 8, a flight flown at the same latitude, but with $[O_3]$ of ~30 ppbv (a more typical value).

In Figure 3 – flight 17, the data at 20:45 UTC show extremely depressed (~2.5 x 10^6 molecule cm^{-3}) concentrations of OH when compared to values measured ten minutes

before or after (~6 x 10^6 molecule cm^{-3}). These lower concentrations were observed during a portion of the flight in which the aircraft flew under a large deck of stratoform clouds. Later at 22:45-23:00, elevated concentrations of OH are observed when compared to the times on either side of the interval. During this portion of the flight, the P-3 flew above a cloud layer located at ~4,500 ft. Elevated concentrations of OH have been observed over clouds in the past by our group [*Mauldin et al.*, 1997, 1998, 1999]. In those works we concluded that the elevated OH concentrations were caused by an increase actinic flux. In contrast to that work, the 20:45 time period demonstrates the ability of a high altitude cloud to lower [OH] by attenuating the actinic flux under it. Figure 7 is a plot of measured and modeled OH together with $j(O_3)$ values determined from the spectral radiometer aboard the aircraft. As can be seen during this time period the value of $j(O_3)$ falls by approximately a factor of 2.5, and the [OH] drops by about a factor 2.4 demonstrating the correlation between OH and $j(O_3)$. During the 22:45-23:00 UTC time period, the $j(O_3)$ increases by ~45%, and the OH increases from ~5 x 10^6 to ~9.5 x 10^6 molecule cm^{-3}. Presumably these increased values arise from increased upwelling radiation from the cloud top combined with slightly increased H_2O above the cloud. The modeled OH again shows good agreement, even during these periods of increased and decreased actinic flux.

4. Conclusions

The SICIMS technique described here allowed a large number of OH, H_2SO_4, and MSA measurements to be performed aboard the NASA P-3B during the PEM-Tropics B study. These measurements are further enhanced by the use of an improved calibration

assembly, which allows reliable calibrations to be performed under low [H_2O] (high altitudes). The use of this improved calibration system has reduced the reported uncertainty of high altitude OH values by a total of 20% (42% vs 62%) compared to values previously reported by our group [*Mauldin et al.*, 1997, 1998]. Additionally, in light of the high altitude calibration values obtained in this study, the high altitude values previously reported by *Mauldin et al.* [1997, 1998] should be lowered by as much as 38% for data obtained at the highest altitudes. These corrections do not apply to data presented here. If corrected values are desired, the reader is directed to contact the authors.

When combined with other parameters measured aboard the aircraft, the OH measurements presented here provide an extensive data set for comparison with model calculations. Overall comparison with the Ga. Tech. photochemical box model simulations yields generally good agreement. The calculated slope of 1.2 shown in Figure 4 indicates that the model has a tendency to predict slightly higher values than measured. As shown in Figure 5, the largest discrepancies of ~60% were observed at the highest altitudes where the [H_2O] generally dropped to less than 1 mb. While this concentration of H_2O is not extremely small, it is nearing the detection limit for the dew point hygrometer aboard the aircraft. If there are errors in the reported [H_2O], a key compound in the production of OH, there will be errors in the [OH] calculated by the model. The above argument is not meant to explain these discrepancies, but to point out the need for accurate measurements of species important in the production of OH when trying to model OH or HO_x photochemistry.

Another highlight of the study was an encounter of an air mass with low O_3 concentrations. During flight 10, boundary layer [O_3] of <5 ppbv were observed as compared to more typical values of 30-40 ppbv. Such a suppression of a compound important in the production of OH is revealed in both measurements and model simulations. The data shown in Figure 6 reveal a midday boundary layer [OH] of ~5 x 10^6 molecule cm^{-3}, a value some 45% lower than the value of 7 x 10^6 molecule cm^{-3} observed during flights flown at the same latitude, but with more typical O_3 concentrations (flight 8). It is interesting to note that while [O_3] is a factor of 6-8 lower than typical levels, the midday [OH] only dropped by a factor of 2. As the production of OH has a square root dependence on ozone concentration, the production of OH is lowered by a factor of ~2-3, which is in the range of the reduction of OH. Model simulations reveal that the OH production terms for boundary layer portions of flight 10 are approximately a factor of 2-2.5 smaller than calculated for flight 8. Thus, while the ozone concentration of the air mass encountered during flight 10 has been reduced significantly, the production level of OH is still maintained at levels to sustain a reasonable oxidizing capacity.

The portion of flight 17 flown around clouds is also of interest. In addition to elevated levels of OH observed in and over clouds previously reported [*Mauldin et al.*, 1997, 1998], here we also report depressed values of OH under a cloud. In Figure 7, it can be seen that [OH] falls from ~6 x 10^6 molecule cm^{-3} observed on either side of the cloud encountered at 20:45 to 3 x 10^6 molecule cm^{-3} observed under it. This decrease in [OH] is due to a decrease in actinic flux, as can be seen by the large change in $j(O_3)$ shown in Figure 7. For the cloud encountered at 22:45-23:00 UTC time period, the OH increased by nearly a factor of two as the aircraft flew above the cloud. Again this change

can be attributed to an increase in actinic flux as indicated by the increase in $j(O_3)$ observed during this time period. Thus, in this single flight the ability of clouds to both increase and decrease OH concentrations is demonstrated. While these changes of OH around clouds are not unexpected, they do raise the question of how clouds impact the column concentration of OH. In light of the present data, it would appear that cloud altitude plays a significant roll in such a calculation. If a cloud were at a lower altitude such as the boundary layer where H_2O concentrations are typically high, it is possible that the reduced concentration of OH produced beneath the cloud is compensated for by enhanced OH production above and inside the cloud leading to either a constant or larger column concentration. If however, the cloud were at a high altitude where H_2O concentrations are typically low, it is possible that the increased OH production above and inside the cloud could be overwhelmed by the reduction in OH production below the cloud leading to a decrease in column [OH]. Thus, depending upon a clouds altitude, it could lead to an increase, decrease, or a redistribution of column OH. Further discussion of the impact of clouds upon OH concentrations will be given in a future publication.

It is also interesting to note that the modeled OH concentrations show generally good agreement, even during the periods of increased and decreased actinic flux. This agreement is much better than the simulations presented in *Mauldin et al.* [1997, 1998] for conditions in and above clouds using either the Ga. Tech model or one developed at the NOAA Aeronomy Lab. These models used as inputs actinic fluxes derived from Eppley radiometer measurements. As stated in *Mauldin et al.* [1987, 1998] actinic fluxes derived in this manner tend to under estimate $j(O_3)$ values. In contrast, the simulations presented here used j values obtained from the spectral radiometer flown aboard the

NASA P-3B. In comparison to the Eppely, which can only measure intensity in a limited wavelength range, this instrument can obtain direct determinations of j values at different photolysis frequencies, an ability that greatly enhances the model derived OH values.

Acknowledgment. The authors wish to thank all of the PEM-Tropics B science team for the use of their data in the model runs. This work was supported through the NASA/GTE program. The National Center for Atmospheric Research is operated by the University Corporation for Atmospheric Research under the sponsorship of the National Science Foundation.

5. References

Atkinson, R., *et al.*, Evaluated kinetic and photochemical data for atmospheric chemistry: Supplement VI, IUPAC subcommittee on gas kinetics data evaluation for atmospheric chemistry, *J. Phys. Chem. Ref. Data*, *26*, 1329-1499, 1997.

Cantrell, C.A., G. Tyndall, and A. Zimmer, Absorption cross-section for water vapor from 183 to 193 nm, *J. Geophys. Res.*, *24*, 2195-2198, 1997.

Creasy, D.J., D.E. Heard, and J.D. Lee, Absorption cross-section measurements of water vapour and oxygen at 185 nm. Implications for the calibration of field instruments to measure OH, HO_2, and RO_2 radicals, *Geophys. Res. Lett.*, *27*, 1651-1654, 2000.

Davis, D.D., G. Chen, A. Bandy, D. Thornton, F. Eisele, L. Mauldin, D. Tanner, D. Lenschow, H. Fuelberg, B. Huebert, J. Heath, A. Clarke, and D. Blake, Dimethyl sulfide oxidation in the equatorial Pacific: Comparison of model simulations with field observations for DMS, SO_2, H_2SO_4(g), MSA(g), MS, and NSS, *J. Geophys. Res.*, *104*,

5765-5784, 1999.

DeMore, W.B., S.P. Sander, D.M. Golden, R.F. Hampson, M.J. Kurylo, C.J. Howard, A.R.Ravishankara, C.E. Kolb, and M.J. Molina, Chemical kinetics and photochemical data for use in stratospheric modeling, *in evaluation 12, JPL Publ. 97-4*, 266 pp., Jet Propul. Lab., Pasadena, Calif., 1997.

Duynkerke, P.G., and M. Van Weele, Actinic fluxes: The role of clouds in photodissociation, *Boundary-Layer Meterol.*, *62*, 417-432, 1991.

Eisele, F.L., and D.J. Tanner, Ion-assisted tropospheric OH measurements, *J. Geophys. Res.*, *96*, 9295-9308, 1991.

Eisele, F.L., and D.J. Tanner, Measurement of the gas phase concentration of H_2SO_4 and methane sulfonic acid and estimates of H_2SO_4 production and loss in the atmosphere, *J. Geophys. Res.*, *98*, 9001-9010, 1993.

Hofzumahaus, A., T. Brauers, U. Aschmutat, U. Brandenburger, H.-P. Dorn, M. Hausmann, M. Heßling, F. Holland, C. Plass-Dülmer, M. Sedlacek, M. Weber, and D. Ehhalt, Reply to comment by *Lanzendorf et al.* [1997], *Geophys. Res. Lett.*, *24*, 3039-3040, 1997.

Hudson, R.D., Absorption cross-sections of stratospheric molecules, *Can. J. Chem.*, *52*, 1465-1478, 1974.

Madronich, S., Photodissociation in the atmosphere 1. Actinic flux and the effects of ground reflections and clouds, *J. Geophys. Res.*, *92*, 9740-9752, 1987.

Mauldin, R.L. III, G.J. Frost, F.L. Eisele, S. Madronich, S.J. Flocke, and A.S.H. Prevot, New insights on OH: Measurements around and in clouds, *Geophys. Res. Lett.*, *24*, 3033-3036, 1997.

Mauldin, R.L. III, D.J. Tanner, G.J. Frost, G. Chen, A.S.H. Prevot, D.D. Davis, and F.L. Eisele, OH measurements during ACE-1: observations and model comparisons, *J. Geophys. Res.*, *103*, 16713-16729, 1998.

Mauldin, R.L. III, D.J. Tanner, G.J. Frost, G. Chen, A.S.H. Prevot, D.D. Davis, and F.L. Eisele, OH measurements during PEM-Tropics A, *J. Geophys. Res.*, *104*, 5817-5827, 1999.

McKeen, S.A., G. Mount, F. Eisele, E. Williams, J. Harder, P. Goldan, W. Kuster, S.C. Liu, K. Baumann, D. Tanner, A. Fried, S. Sewell, C. Cantrell, and R. Shetter, Photochemical modeling of hydroxyl and its relationship to other species during the tropospheric OH photochemistry experiment, *J. Geophys. Res.*, *102*, 6467-6493, 1997.

Tanner, D.J., A. Jefferson, and F.L. Eisele, Selected ion chemical ionization mass spectrometric measurement of OH, *J. Geophys. Res.*, *102*, 6415-6425, 1997.

Yoshino, K., J.R. Esmond, W.H. Parkinson, K. Ito, and T. Matsui, Absorption cross section of water vapor in the wavelength region 120 to 188 nm, *Chem. Phys.*, *211*, 387-391, 1996.

Wang, L., *et al.*, Analysis of HO_x chemistry in the tropics as derived from PEM-Tropics B observations, *J. Geophys. Res.*, This Issue.

Figure Captions

Figure 1. Schematic diagram of the SICIMS instrument used for the airborne measurement of OH, H_2SO_4, and MSA during the PEM-Tropics B study. The inset shows the new calibration source, which allows better calibrations to be performed under low H_2O concentrations (high altitudes).

Figure 2. Plot of calibration coefficient versus pressure altitude obtained during the PEM-Tropics B study. Measurements and calibrations were performed under two different electro-static lens settings. As can be seen with the 700 mb values, these settings affect the obtained value for the calibration coefficient. Also shown are linear fits to the values for each lens setting. Depending on the lens setting recorded, the appropriate fit was used to obtain the OH concentrations presented here (see text).

Figure 3. Concentrations of OH measured during each flight during the PEM-Tropics b study. Also shown for reference is an altitude profile for each flight. Data are presented as 30 s measurements, which are the result of 8 s of OH signal measurement, and 8 s of OH background measurement during each 30 s period (see text).

Figure 4. Comparison of measured OH values from the entire PEM-Tropics B study with those obtained using the Ga. Tech. photochemical box model. Also shown is the line indicating 1:1 correlation between the values. A linear fit yields a slope of 1.26,

indicating a slight tendency for the model to over-predict OH concentrations when compared to the measured values presented here.

Figure 5. Plot of measured and modeled [OH] for P-3 flight 14. Also shown for reference are an altitude profile, and the values of $j(O_3)$ and $[H_2O]$. The agreement between modeled values and measurements is generally good with the largest deviations occurring at high altitudes. The last portion of the flight was flown at night. Note the precision in measuring low OH concentrations. Five-minute averages during this time period yield values of $(3\text{-}5 \pm 10) \times 10^4$ molecule cm^{-3}.

Figure 6. Plot of measured and modeled OH for P-3 flight 10. Also shown for reference are an altitude profile and the measured $[O_3]$. Note the low ozone concentrations observed in the boundary/buffer layer runs. Model simulations show that the OH production in these regions are ~2-2.5 times smaller than those calculated for flight 8, a flight flown at approximately the same latitude, but in which more typical $[O_3]$ were observed.

Figure 7. Plot of measured and modeled OH for P-3 flight 17. Also shown for reference are an altitude profile and the measured $j(O_3)$. Time periods where the aircraft encountered clouds are marked. Note the large decrease in OH observed as the aircraft passed beneath the cloud at 20:45. A large increase in OH is observed as the aircraft flew above a cloud at 22:45-23:00. This flight demonstrates the ability of clouds to both increase and decrease OH concentrations. Also note the good

agreement of measured and modeled OH values, even during the periods of increased and decreased actinic flux.

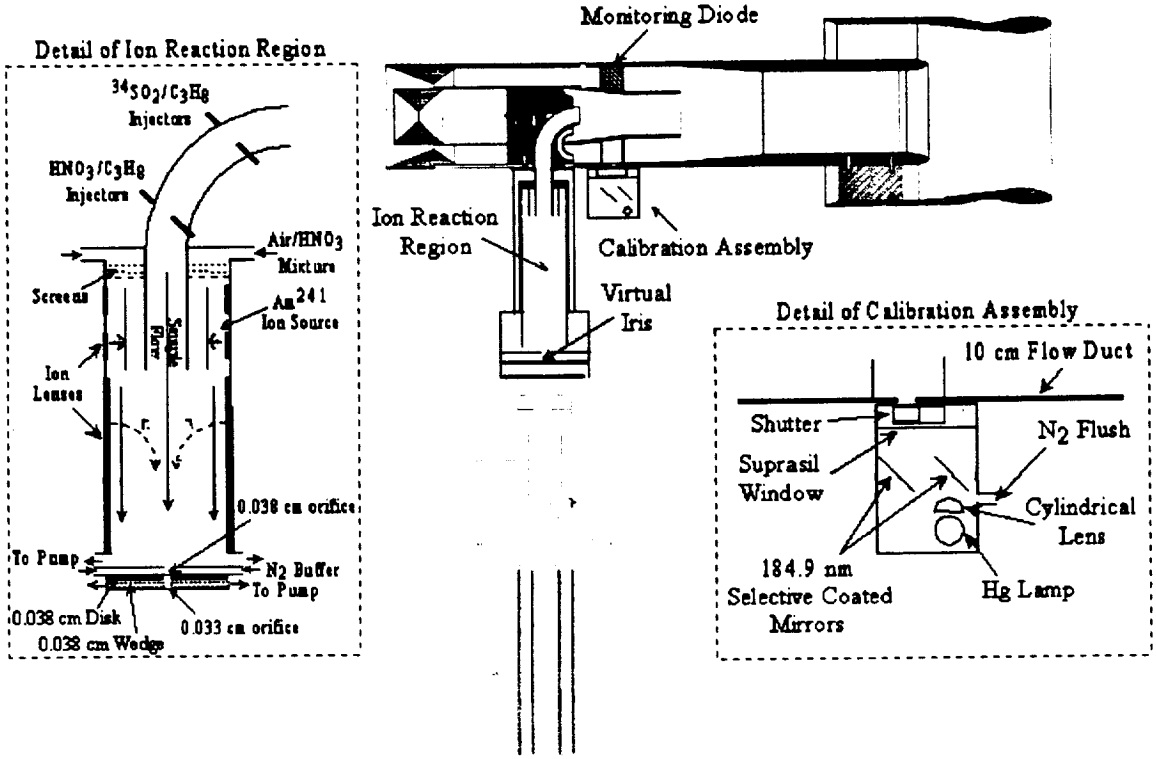
Detail of Ion Reaction Region
$^{34}SO_2/C_3H_8$ Injectors
HNO_3/C_3H_8 Injectors
Air/HNO_3 Mixture
Screens
Am^{241} Ion Source
Ion Lenses
0.038 cm orifice
To Pump
N_2 Buffer
To Pump
0.038 cm Disk
0.038 cm Wedge
0.033 cm orifice
Monitoring Diode
Ion Reaction Region
Calibration Assembly
Virtual Iris
Detail of Calibration Assembly
10 cm Flow Duct
Shutter
N_2 Flush
Suprasil Window
Cylindrical Lens
184.9 nm Selective Coated Mirrors
Hg Lamp

Figure 1

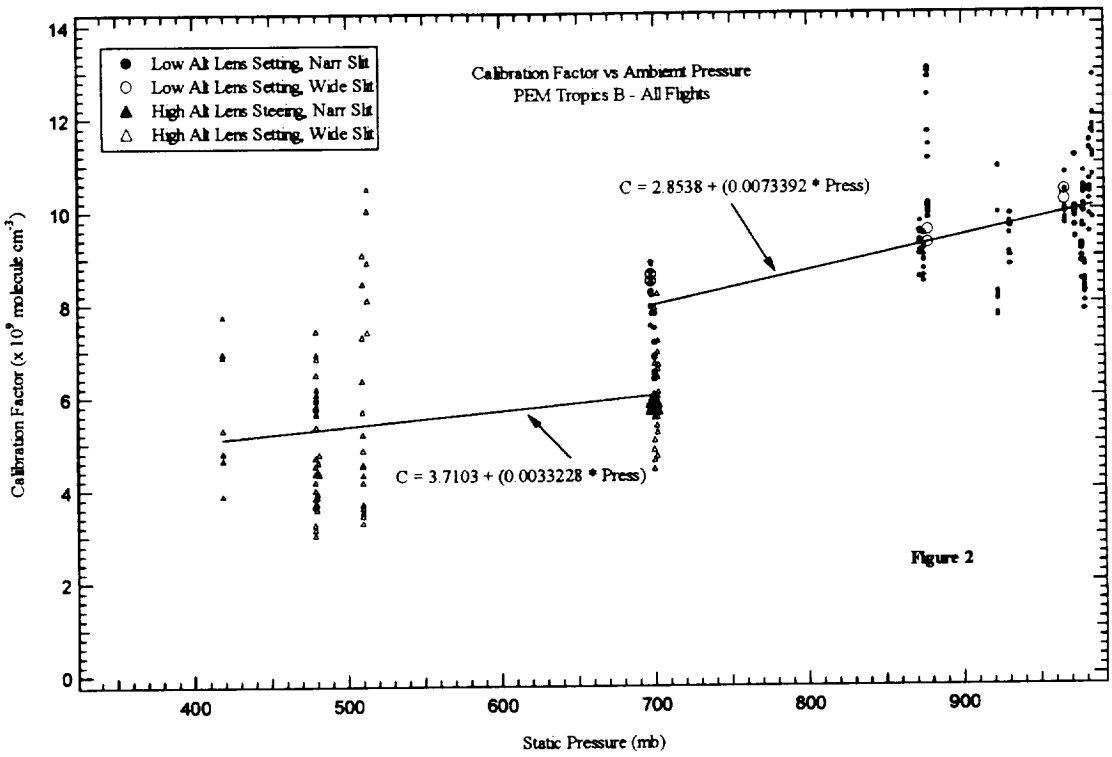
Low Alt Lens Setting, Narr Slit
Low Alt Lens Setting, Wide Slit
High Alt Lens Steering, Narr Slit
High Alt Lens Setting, Wide Slit
Calibration Factor vs Ambient Pressure
PEM Tropics B - All Flights
C = 2.8538 + (0.0073392 * Press)
C = 3.7103 + (0.0033228 * Press)
Calibration Factor (x 10^9 molecule cm^-3)
Static Pressure (mb)
0
2
4
6
8
10
12
14
400
500
600
700
800
900

Figure 2

Figure 3

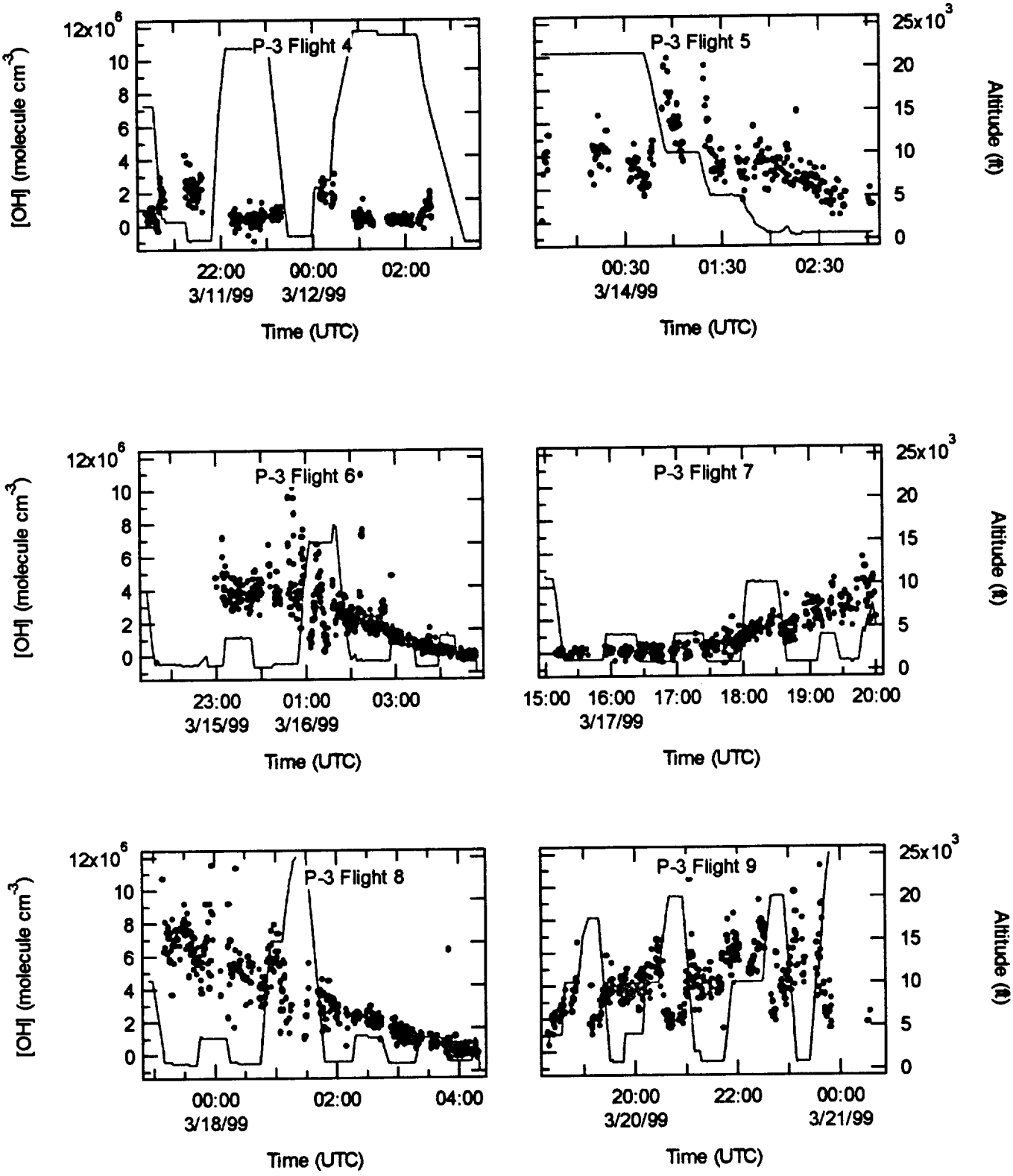
P-3 Flight 4
P-3 Flight 5
P-3 Flight 6
P-3 Flight 7
P-3 Flight 8
P-3 Flight 9
[OH] (molecule cm-3)
12x10^6
25x10^3
Altitude (ft)
Time (UTC)
22:00
3/11/99
00:00
3/12/99
02:00
00:30
3/14/99
01:30
02:30
23:00
3/15/99
01:00
3/16/99
03:00
15:00
3/17/99
16:00
17:00
18:00
19:00
20:00
00:00
3/18/99
02:00
04:00
20:00
3/20/99
22:00
00:00
3/21/99

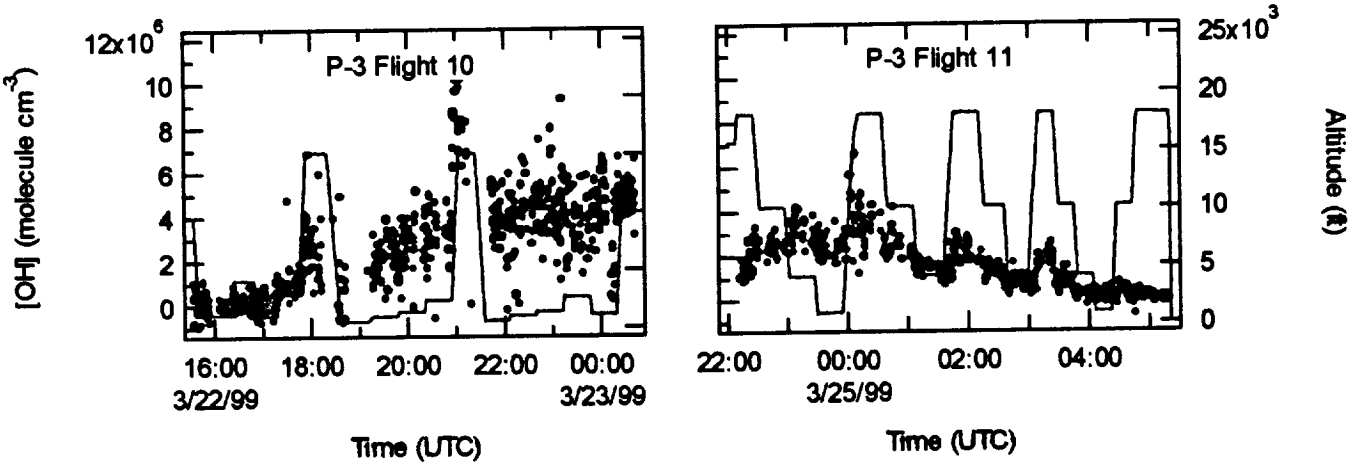
P-3 Flight 10
[OH] (molecule cm-3)
12x10^6
10
8
6
4
2
0
16:00
3/22/99
18:00
20:00
22:00
00:00
3/23/99
Time (UTC)
P-3 Flight 11
25x10^3
20
15
10
5
0
Altitude (ft)
22:00
00:00
3/25/99
02:00
04:00
Time (UTC)

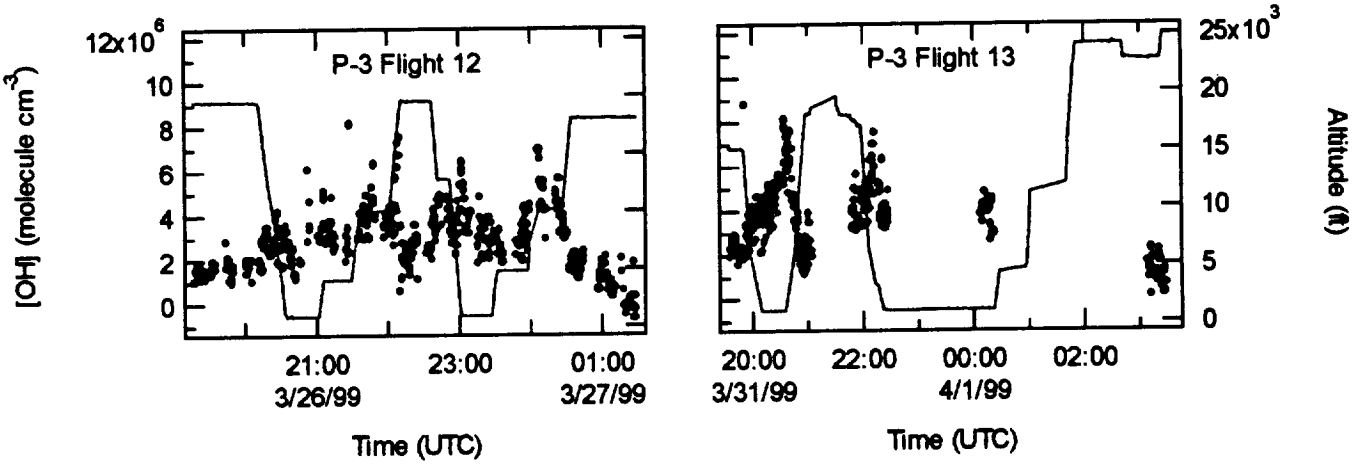
P-3 Flight 12
[OH] (molecule cm-3)
12x10^6
10
8
6
4
2
0
21:00
3/26/99
23:00
01:00
3/27/99
Time (UTC)
P-3 Flight 13
25x10^3
20
15
10
5
0
Altitude (ft)
20:00
3/31/99
22:00
00:00
4/1/99
02:00
Time (UTC)

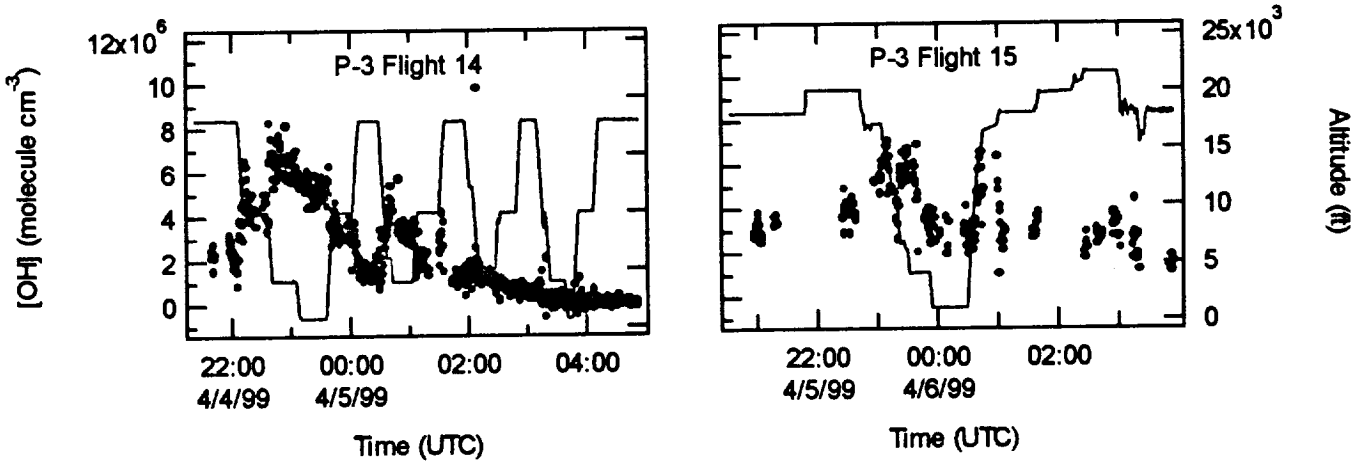
P-3 Flight 14
[OH] (molecule cm-3)
12x10^6
10
8
6
4
2
0
22:00
4/4/99
00:00
4/5/99
02:00
04:00
Time (UTC)
P-3 Flight 15
25x10^3
20
15
10
5
0
Altitude (ft)
22:00
4/5/99
00:00
4/6/99
02:00
Time (UTC)

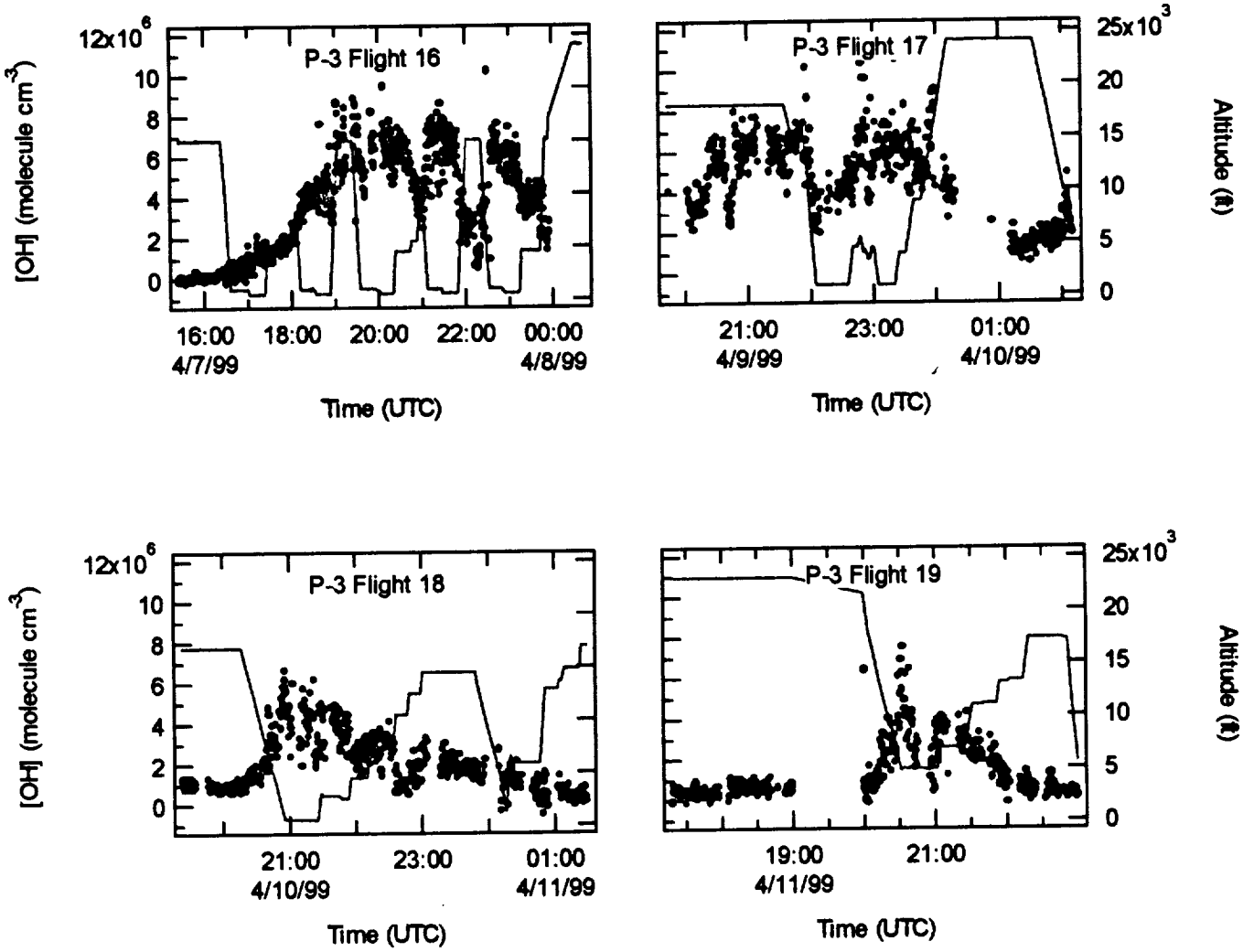
P-3 Flight 16
P-3 Flight 17
P-3 Flight 18
P-3 Flight 19
[OH] (molecule cm-3)
Altitude (ft)
Time (UTC)
12x10^6
25x10^3
16:00 4/7/99
18:00
20:00
22:00
00:00 4/8/99
21:00 4/9/99
23:00
01:00 4/10/99
21:00 4/10/99
01:00 4/11/99
19:00 4/11/99

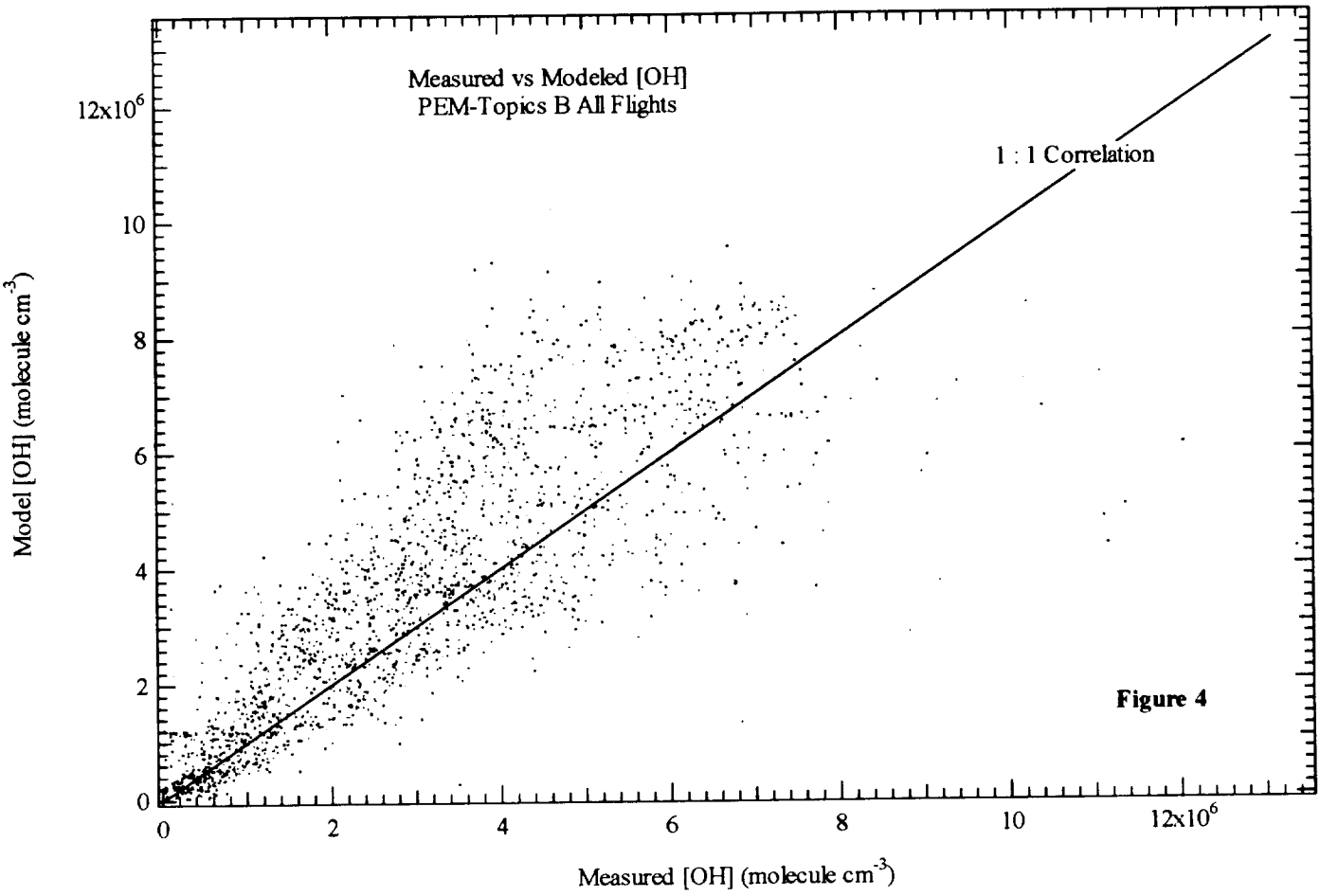
Measured vs Modeled [OH]
PEM-Topics B All Flights
1 : 1 Correlation
Model [OH] (molecule cm-3)
Measured [OH] (molecule cm-3)
0
2
4
6
8
10
12x10^6

Figure 4

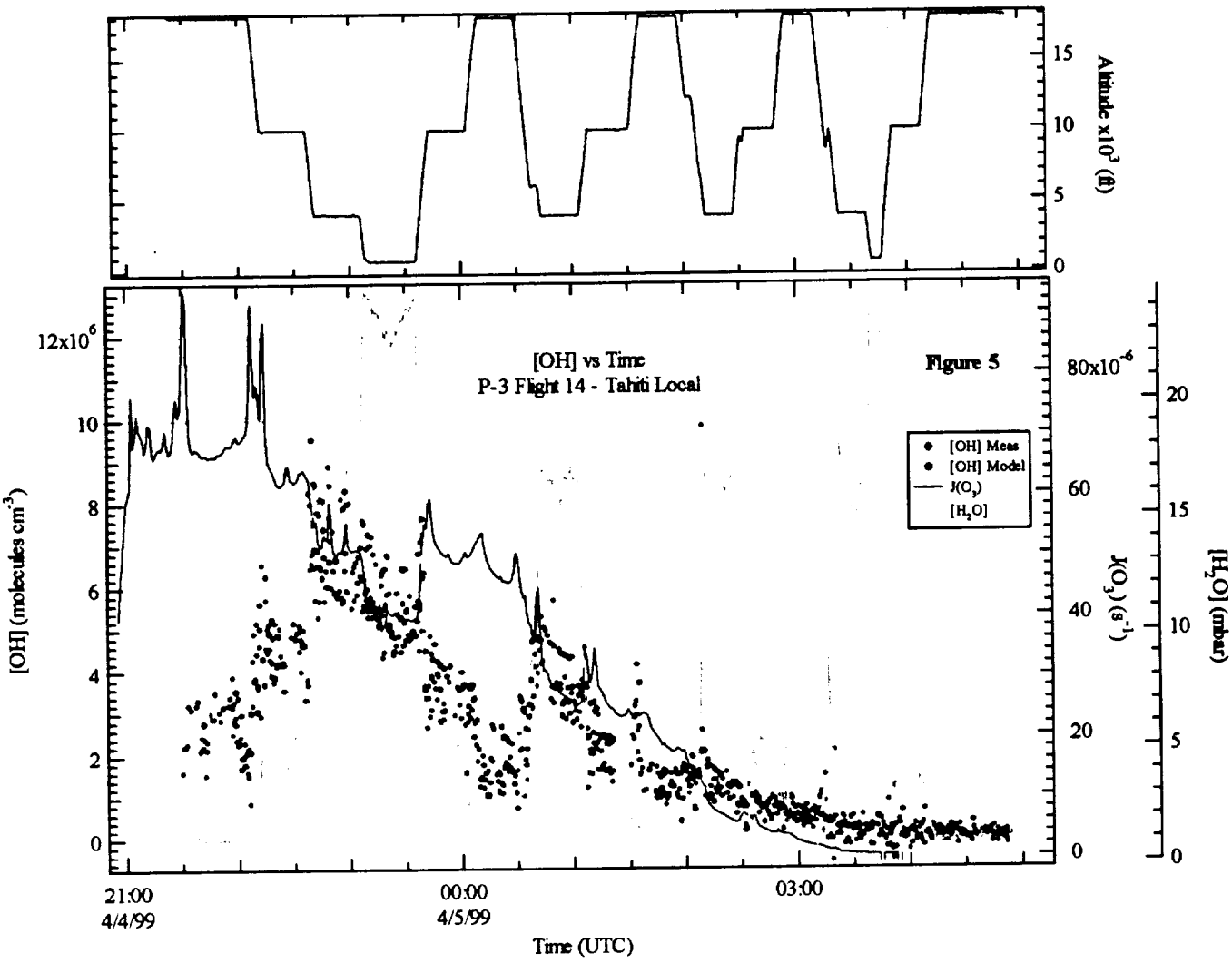
Altitude x10^3 (ft)
15
10
5
0
[OH] vs Time
P-3 Flight 14 - Tahiti Local
Figure 5
[OH] Meas
[OH] Model
J(O$_3$)
[H$_2$O]
[OH] (molecules cm^{-3})
12x10^6
10
8
6
4
2
0
80x10^{-6}
60
40
20
0
J(O$_3$) (s^{-1})
20
15
10
5
0
[H$_2$O] (mbar)
21:00
4/4/99
00:00
4/5/99
03:00
Time (UTC)

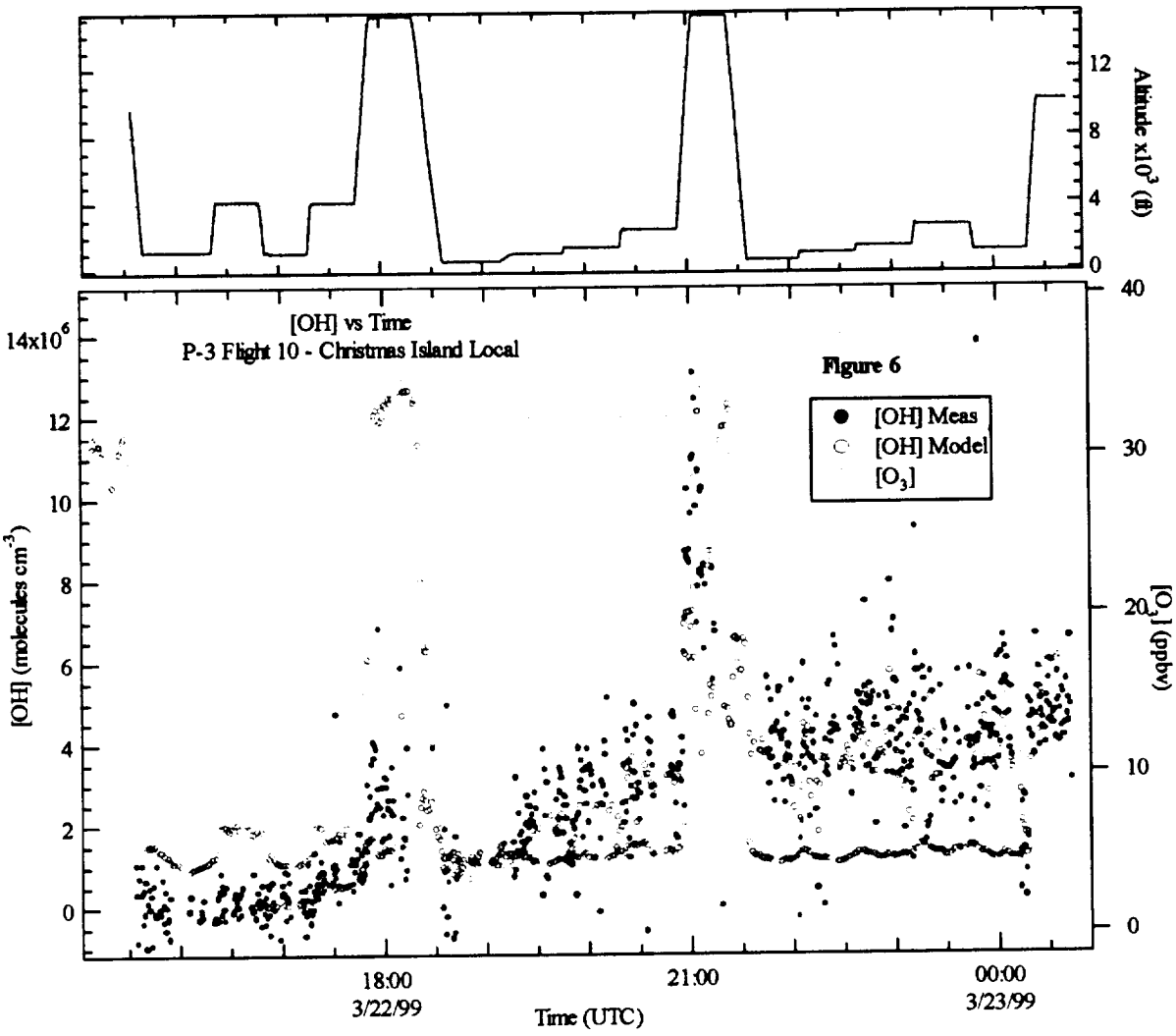
[OH] vs Time
P-3 Flight 10 - Christmas Island Local
Figure 6
[OH] Meas
[OH] Model
[O3]
[OH] (molecules cm-3)
14x10^6
[O3] (ppbv)
Altitude x10^3 (ft)
18:00
3/22/99
21:00
00:00
3/23/99
Time (UTC)

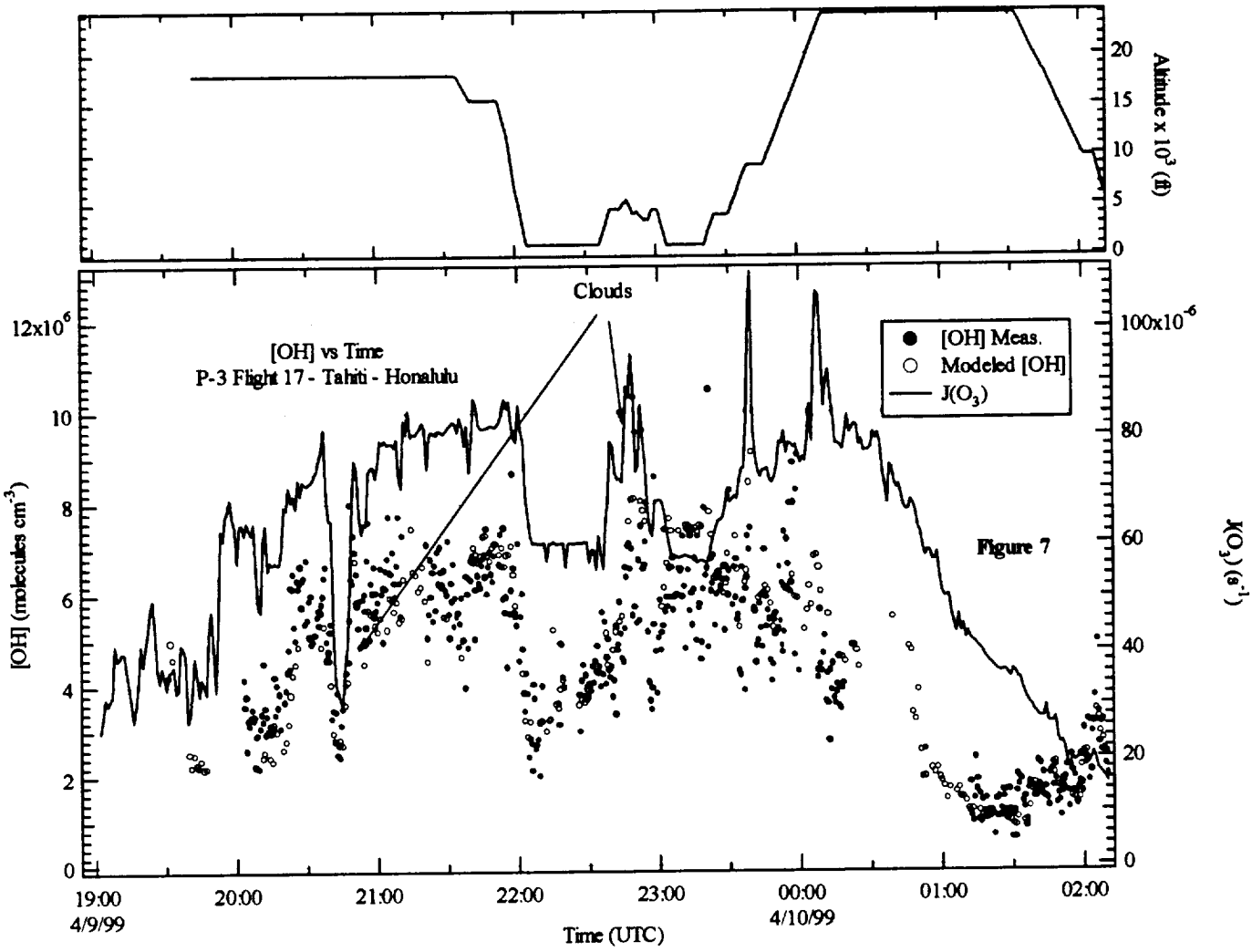
Altitude x 10^3 (ft)
20
15
10
5
0
Clouds
[OH] vs Time
P-3 Flight 17 - Tahiti - Honalulu
[OH] Meas.
Modeled [OH]
J(O3)
12x10^6
10
8
6
4
2
0
100x10^-6
80
60
40
20
0
[OH] (molecules cm^-3)
J(O3) (s^-1)
19:00
4/9/99
20:00
21:00
22:00
23:00
00:00
4/10/99
01:00
02:00
Time (UTC)

Figure 7

APPENDIX D

The Relationship Between OH Measurements on Two Different NASA Aircraft During PEM-Tropics B

F. L. Eisele, R. L. Mauldin, D. J. Tanner, C. Cantrell, E. Kosciuch, J. B. Nowak, B. Brune, I. Faloona, D. Tan, D. D. Davis, L. Wang, and G. Chen

Abstract. OH measurements were performed on both the P3-B and the DC-8 aircraft throughout PEM-Tropics B, using two very different measurement techniques. While no direct comparison was possible because of the difference in flight paths of the two aircraft, 2 brief measurement periods in close proximity allow at least a glimpse of how the two measurements compare. The first comparison took place in the marine boundary layer and showed exceptionally good agreement between the two aircraft OH measurements. The second set of close proximity flights at 5.5 km altitude resulted in an average concentration difference approximately equal to the uncertainty limit associated with either individual instrument, but much less than the combined uncertainties from all the contributing measurements. In both cases the comparisons were made by normalizing the data with a photostationary state model. In addition, a comparison of the OH concentrations measured by each aircraft from 25 degrees north latitude to 25 degrees south latitude over the entire longitude and altitude range of the mission resulted in agreement within about 10% but with a trend of higher DC-8 /P-3B OH ratios at higher altitudes. While a definitive comparison of these two OH instruments must await a far

more rigorous future test, the present results show that there were no clear OH measurement discrepancies observed. The dramatic differences in these two measurement techniques also minimizes the chance of common interferences or calibration errors.

1. Introduction

The hydroxyl radical is the primary cleansing agent of the lower atmosphere. It is initially derived from the photolysis of ozone to form $O(^1D)$ and its subsequent reaction with water to yield two OH radicals. Once formed, OH reacts with most compounds emitted into the atmosphere, including virtually all hydrocarbons and their oxidation products and most sulfur and nitrogen containing compounds. Depending on the specific reaction, OH will either be destroyed as, for example, when it reacts with NO_2 to form HNO_3; or recycled, as when it reacts with CO or methane to form HO_2 or RO_2. The highly reactive nature of OH makes it difficult to measure and to model for several reasons. In the case of measurements it can react with relatively stable and abundant gases such as CO and methane, thus its lifetime is short, on the order of a second, and its peak concentrations are typically held very low, i.e., in the 10^6 molecules cm^{-3} range. Measurements must therefore be accomplished quickly, sensitively, and without significant new reaction possibilities such as contact with inlet or sample tube walls. On the modeling side, the primary source of OH is fairly well established, at least at low altitudes, but the sinks include CO, methane, plus small amounts of numerous other compounds. Many of the reaction rates with these other compounds are unknown, their concentrations are often not measured, and their reaction products are also often in question. There are also several secondary sources of OH which involve various forms of chemical and photolytic recycling through compounds such as HO_2, H_2O_2 and their organic counterparts.

Despite measurement difficulties, it is critical that OH be accurately measured because it is the concentration of this radical that directly controls the lifetime of most biogenic and anthropogenic emissions. It is also important that models accurately portray the role of various parameters in controlling OH concentrations if the consequences of changes in anthrogenic or biogenic emissions are to be properly understood. Before model/measurement comparisons can be meaningfully discussed, however, it must first be determined how models compare with each other (which is beyond the scope of this paper) and how measurements on the two aircraft compare. It is the purpose of this paper to provide some new insight into the level of agreement between the two aircraft OH measurement instruments used in PEM-Tropics B. The authors will be the first to admit that the data to be discussed does not constitute a rigorous intercomparison. It is, however, important to use the limited data set in which OH was measured on both aircraft at similar locations and times to make sure that agreement between the two very different OH measurement techniques is at least sufficient to allow meaningful comparisons of the photochemical results from the NASA DC-8 and P-3B aircraft. If the two OH instruments consistently differ by more than their combined limits of uncertainty when measuring under apparently similar conditions, then clearly the interpretation of measurement/model comparisons would be very different, depending on which aircraft platform the data came from. If, on the other hand, measurements typically agree within the limits of uncertainty of each instrument, then there is at least no a priori expectation that measurement/model interpretations are platform dependent. This does not mean that the two instruments can be said to agree or even that they are not both wrong. A statement of such agreement or lack thereof awaits a far more rigorous intercomparison.

The possibility of both instruments being biased in the same way or containing similar interferences may be even more difficult to completely rule out. These two techniques, however, are so different in operating pressure, analytical methods, and ion or photon detection that it would be difficult to conceive of a mechanism or chemical interference that might be responsible for a common bias in both instruments.

2. Instrumentation and Measurement Techniques

The instrumentation used to measure OH on the DC-8 and P-3B could not be much more dissimilar. The DC-8 instrument uses laser induced fluorescence (LIF) to preferentially excite OH molecules and then employs photon counting to detect fluorescent photons emitted by the excited OH molecules after a brief time delay. The measurements take place at a reduced pressure of only a few torr, which is achieved by rapid pumping of sampled air through a critical orifice. The aircraft inlet design is unique to this instrument and is well-modeled. Calibration is achieved by generating a known concentration of OH via several laboratory techniques including H_2O photolysis at 184.9 nm and measuring them at a range of internal pressures from about 0.3 to 1.0 kp. This pressure range corresponds to that in the measurement cell at maximum flight altitude and sea level respectively.. Relative changes in detection sensitivity are also monitored using 184.9 nm photolysis of H_2O in flight. The DC-8 instrument is located in the forward belly of the aircraft and samples air directly below the fuselage. Measurements are typically made at mach 0.7 ± 0.1 and altitudes of 15,000 feet to 41,000 feet, with profiles down to the ground.

The P-3B instrument uses chemical titration of ambient OH with $^{34}SO_2$ to produce $H_2{}^{34}SO_4$ which is subsequently measured by selected ion chemical ionization mass spectrometry (SICIMS) using NO_3^- reactant ions. The titration and chemical ionization takes place essentially at ambient pressure and temperature, and only after the ion chemistry is completed are the ions sampled through a N_2 sheath gas into a high vacuum environment where they are mass analyzed. Detection is by single ion counting and OH concentrations are derived from the ratio of $H^{34}SO_4^-$ and NO_3^- ion count rates which leads to a very stable calibration coefficient. Calibration is achieved in situ in ambient air by photolyzing a known concentration of H_2O in the inlet at a known velocity with a known photon flux at 184.9 nm photons. The inlet design used by this instrument is also unique to this application and has undergone extensive wind tunnel testing. The P-3B instrument samples near the front of the aircraft on the port side at window height. Measurements are typically made at mach 0.3±0.1 at altitudes of 300 feet to 25,000 feet with a focus on boundary layer studies. Far more detailed descriptions of the DC-8 LIF instrument [*Stevens et al.*, 1994; *Mather et al.*, 1997; *Brune et al.*, 1998; *Tan et al.*, 1998; and *Faloona et al.*, 2000] and the P-3B SICIMS instrument [*Eisele and Tanner*, 1991; *Tanner and Eisele*, 1995; *Eisele et al.*, 1996; *Eisele et al.*, 1997; *Mount et al.*, 1997] have been published previously, and the PEM-Tropics B results from this technique are included in this special issue.

The similarities between these two instruments are few. They both have fairly similar detection sensitivities and in each case this is achieved by counting discrete events: i.e., the detection of individual photons or ions. Absolute measurement uncertainties are similar (about ± 40%), as is the use of 184.9 nm photolysis of H_2O as a

calibration standard. Both instruments have also participated in several previous aircraft and ground based studies [*Eisele and Tanner*, 1991; *Eisele et al.*, 1994, 1996; *Tanner et al.*, 1997; *Jefferson et al.*, 1998; *Mauldin et al.*, 1998, 1999; *Mather et al.*, 1997; *Brune et al.*, 1998; *Tan et al.*, 1998; and *Faloona et al.*, 2000]. Apart from these functional similarities, the two instruments are profoundly different. The DC-8 instrument uses electronic excitation of OH via photo absorption at 308 nm and the detection of the subsequent resonance fluorescence to detect OH molecules. The P3-B alternatively makes use of the chemical reactivity of OH with SO_2 to form a product which is preferentially detected because of its high acidity and specific molecular mass. Thus, in order for these two instruments to have a common interfering species that could be mistaken for OH in each, this compound would need to have an electronic excitation level similar to OH, form a high acidic compound with $^{34}SO_2$, and result in an ion with the same mass as $H^{34}SO_4^-$. Other differences include operating pressures. The DC-8 instrument samples air through an orifice into a low pressure region (about 0.4-1.1 kp) where the LIF detection if accomplished. On the P-3B, the chemical reactions used to detect OH are all accomplished at pressures slightly above ambient due to ram air pressure in the inlet. The resulting ions are sampled into the low pressure mass analysis region only after the reactions are stopped by passing the ions through a N_2 buffer gas just in front of the vacuum entrance aperture. The transition from ambient to low pressure is therefore also quite different, in one case being in air and involving the OH radical directly and in the second being in dry N_2 and involving NO_3^- and HSO_4^- ions. Again, the opportunity for water vapor, temperature, pressure or some trace gas to affect both of these compounds in the same way during the pressure reduction phase is not

likely. The two instruments each have unique inlets, however, they both slow the sampled air flow significantly compared to free stream flow. The DC-8 operates at speeds up to about twice those of the P-3B, and as a result DC-8 ram air pressure and air temperature rises are about a factor of 3 to 4 times those in the P-3B inlet. As mentioned in the introduction, calibration methodology is also quite different, though both instruments do use 184.9 nm photolysis of H_2O for determining a calibration factor.

3. Measurement Results

PEM-Tropics B was not intended to provide an intercomparison of measurement techniques on the DC-8 and P-3B aircraft. The two aircraft were intended to complement each other and not to fly redundant measurement patterns. As a result, there were few instances, where the two aircraft flew in a similar location at a similar time and probably none in which they actually flew through the same air mass. There were, however, two instances on flight #6 on the P-3B and flight #8 on the DC-8 and on flight #14 on the P-3B and flight #16 on the DC-8) in which similar air masses could have been sampled. The first potential overlap was near Christmas Island, when the DC-8 flew at the same altitude through a similar geographical location to that sampled an hour earlier by the P-3B. Table 1 shows a comparison of measurement times, locations, photolysis rates and the average concentrations of several compounds associated with either OH production or loss measured on the P-3B and DC-8. Most of the compounds measured on the two aircraft look quite similar except NO, which is on average 4 times higher on the P-3B than the DC-8. NO measurements on both aircraft, however, involved concentration spikes that were also reflected in the OH concentration. This suggests that while the air

masses are fairly similar in several respects they are not really the same. More than a factor of 2 difference in average $JO(^1D)$ (but much less in $J(NO_2)$) also suggests that a direct comparison of measurements from the two aircraft is not possible. Rather than trying to correct for differences in individual parameters, a model will be used as a transfer standard. The model is a photochemical box model containing full HO_x-NO_x-CH_4 chemistry and parameterized NMHC chemistry. This model has been previously described in detail by *Crawford et al.* [1999]. Instead of comparing measured OH concentrations directly, the ratio of measured to modeled OH on each aircraft is compared. Since the measurement conditions were quite similar for the two aircraft, the use of a model as a transfer standard should introduce little additional uncertainty due to uncertainties in the reaction and photolysis rates used. The uncertainties associated with the measurement of the most important photochemical parameters on each aircraft do, however, directly contribute to the uncertainty of the comparison. Table 1 also shows the average measured OH concentrations and the ratio of measured to modeled OH for each aircraft. Figure 1 shows the temporal dependence of the data sets from both aircraft. Note that there are spikes in both data sets, making comparison even less certain. The very high level of agreement of average measurement/model OH ratios shown in Table 1 has little significance since calibration uncertainties are much larger. Clearly, however, agreement is very good and it is comforting to see that both instruments and models appear to consistently track each other well within the combined uncertainty limits of the measurements and model inputs. In this boundary layer comparison, both measured OH concentrations seem to indicate that modeled values are consistently low by about 30%.

This has only limited significance, since it is within the uncertainty of the OH measurements.

A second opportunity for comparing DC-8 and P-3B OH measurements occurred on a flight out of Tahiti at an altitude of about 5.5 km. In this case, the P-3B flew through an exceptionally uniform air mass 5 times from about noon until late afternoon, local time. The DC-8 flew through nearly the same location and at the same altitude in the mid-afternoon. A comparison of time, location and measured parameters is given in Table 2. While the mixing ratios of O_3, CO and H_2O were fairly consistent between both successive P-3B measurements and the DC-8 measurements, average NO was again higher on the P-3B, this time by a factor of about 2. CH_2O and H_2O_2 also varied by up to a factor of 2 on both P-3B sampling legs. This suggests that the two aircraft were sampling somewhat similar but still not the same air mass. Figure 2 also shows the time sequence of OH measurements made by the two aircraft. Several of the P-3B and the DC-8 data show significant structure in both the measurement and modeled OH concentrations, again making comparisons more difficult. At this 5.5 km altitude comparison, measured-to-modeled OH ratios were quite different for the P-3B and DC-8. An average of the first three or four P-3B measurement/model ratios is about 0.65, compared to a ratio of 1.05 on the DC-8. Thus, the P-3B ratio was 62% of the DC-8 ratio. The uncertainty in the OH measurements is about 40% for either OH instrument and the other measurements used in model calculation on the two different aircraft probably add an additional 15-20% uncertainty per platform to the comparison uncertainty. Much of the latter uncertainty comes from uncertainties in NO concentrations which were measured close to the detection limit. Compounds with

longer lifetimes such as CO and O_3 can generally be measured more accurately and appear to be quite similar when measured by both aircraft. The actinic flux measurements also have relatively small quoted uncertainties and measurements were made on both aircraft with essentially identical instruments. Therefore the observed disagreement in OH between the two aircraft is well within the combined instrumental uncertainty. It is even within or very close to the uncertainty imposed by the sum of the errors from either platform individually. Thus, the present result does not suggest a discrepancy between these two instruments. Neither, however, does the data suggest consistent agreement. With variations in both measured and modeled OH of about a factor of 2 within several individual flight tracks, and with variations of a factor of 2 in the average concentration of short-lived compounds such as NO between the two aircraft, it is not at all clear that the same air mass is being sampled. Thus, the comparisons of the ratio of measured/modeled OH for similar conditions (as determined by other measured photochemical parameters) provides additional evidence that the two instruments are measuring the same compound and that at least in these two situations they agree well within their combined uncertainty limits. These results are also consistent with previous ground-based intercomparison results for these two techniques [*Mount et al.*, 1997 and *Hofzumahaus et al.*, 1998]. For these two aircraft comparison periods, however, it is not clear that only close spatial and temporal proximity of the aircraft added significant new insight into how well the measurement techniques compare. Unless the two aircraft fly side by side for 10 or 20 minutes, and are truly co-located it is unlikely that proximity provides significant benefits. Since this was not the case in PEM-Tropics B, another alternative is to try to compare the bulk measured OH data ratio over a very large area.

Davis et al., this issue, have sorted the OH data from the P-3B and DC-8 into altitude and latitude bins. They have used relatively clear sky measurements and adjusted them for diurnal changes in actinic flux to produce a map of OH concentrations expected at local noon in each of these bins. Averaging the median data from each latitude block common to both aircraft missions (which includes all longitudes) and dividing DC-8 diurnally adjusted OH data by P-3B diurnally adjusted OH data produces the altitude dependent OH measurement ratio shown in Figure 3. While the OH ratios largely stay within the uncertainty bounds of either instrument, a clear altitude trend is observed. The significance of Figure 3, however, should be evaluated in light of several issues. The highest OH ratio corresponds to a very limited latitude range at the highest P-3B altitude. The DC-8 measurements extended much further to both the east and west than did those of the P-3B. Finally, the altitude dependence of OH measurements on each aircraft may contain different biases. The DC-8 flies at low altitudes typically as part of a vertical profile in a selected area. The P-3B spends most of its time involved in low altitude studies and typically chooses high altitude flight paths to optimize transit time.

4. Conclusions

Intercomparing instruments on two very different aircraft can pose substantial difficulties. Differences in air speeds, operating altitudes, modification of airflow by the air frame, and the dangers of flying too close together or in the wake of another aircraft all add to these problems. The large number of diverse instrument types operated on the two aircraft by many different investigators, makes comparative data interpretation even more susceptible to error. This paper provides some insight into the relation between OH

measurements on the P-3B and DC-8 aircraft but a far better comparison is needed. Fairly consistent agreement well with the combined uncertainties of the two instruments provide some evidence that measurement/model comparison on both aircraft are providing useful new insights. DC-8/P-3B OH ratios of about 1.5 at higher altitudes both in adjacent flight paths and in the averages shown in Figure 3, however, suggests the need for a better means of intercomparison at several different altitudes in the future.

After looking at the two sets of adjacent flight track data it also appeared that a comparison of all short and intermediate lifetime species could be highly enlightening. It is clear, however, that unless the two aircraft fly much closer together in space and time (maybe side-by-side within 1-2 km at altitudes where this is possible), that general proximity offers little assurance of flying in the same air mass. To critically compare multi-aircraft measurements there needs to be some assurance that the same air mass is being sampled and this requires more than just similar concentrations of long lived compounds and j values. Flights sufficiently close that they both observe spikes or perturbations with similar relative concentration changes, and spatial extent would, however, help provide evidence for a similar sampling environment. Direct comparison of similar measurements on the same aircraft would, of course, provide the best means of comparing instrument operation.

Acknowledgment. The authors wish to thank all of the other PEM-Tropics B participants for the use of their data in the model runs. This work was supported through the NASA/GTE program. The National Center for Atmospheric Research is operated by the University Corporation for Atmospheric Research under the sponsorship of the National Science Foundation.

References

Brune, W. H., I. C. Faloona, D. Tan, A. J. Weinheimer, T. Campos, B. A. Ridley, S. A. Vay, J. E. Collins, G. W. Sachse, L. Jaeglé, and D. J. Jacob, Airborne in-situ OH and HO_2 observations in the cloud-free troposphere and lower stratosphere during SUCCESS, *Geophys. Res. Lett.*, *25*, 1701-1704, 1998.

Crawford, J., D. Davis, J. Olson, G. Chen, S. Liu, G. Gregory, J. Barrick, G. Sachse, S. Sandholm, B. Heikes, H. Singh, and D. Blake, Assessment of upper tropospheric HO_x sources over the tropical Pacific based on NASA GTE/PEM data: Net effect on HO_x and other photochemical parameters, *J. Geophys. Res.*, *104*, 16,255-16,273, 1999.

Davis, D., G. Grodzinsky, G. Chen, B. Dinunno, F. Eisele, L. Mauldin, D. Tanner, C. Cantrell, W. Brune, D. Tan, *et al.*, Pacific Ocean latitude/altitude distributions: Comparison of observations with model predictions, *J. Geophys. Res.*, this issue.

Eisele, F. L., and D. J. Tanner, Ion assisted tropospheric OH measurement, *J. Geophys. Res.*, *96*, 9295-9308, 1991.

Eisele, F. L., G. H. Mount, F. C. Fehsenfeld, J. Harder, E. Marovich, J. Roberts, M. Trainer, and D. J. Tanner, Intercomparison of tropospheric OH and ancillary trace gas measurements at Fritz Peak Observatory, Colorado, *J. Geophys. Res.*, *99*, 18,605-18,626, 1994.

Eisele, F. L., D. J. Tanner, C. A. Cantrell, and J. G. Calvert, Measurements and steady state calculations of OH concentrations at Mauna Loa Observatory, *J. Geophys. Res.*, *101*, 14,665-14,679, 1996.

Eisele, F. L., R. L. Mauldin III, D. J. Tanner, J. R. Fox, T. Mouch, and T. Scully, An inlet sampling duct for airborne OH and sulfuric acid measurements, *J. Geophys. Res.*, *102*, 27,993-28,002, 1997.

Faloona, I., D. Tan, W. H. Brune, L. Jaeglé, D. J. Jacob, Y. Kondo, M. Koike, R. Chatfield, R. Pueschel, G. Ferry, G. Sachse, S. Vay, B. Anderson, J. Hannon, and H. Fuelberg, Observations of HO_x and its relationship with NO_x in the upper troposphere during SONEX, *J. Geophys. Res.*, *105*, 3771-3783, 2000.

Hofzumahaus, A., U. Aschmutat, U. Brandenburger, T. Brauers, H.-P. Dorn, M. Hausmann, M. Heßling, F. Holland, C. Plass-Dülmer, and D. H. Ehhalt, Intercomparison of tropospheric OH measurements by different laser techniques during the POPCORN campaign 1994, *J. Atmos. Chem.*, *31*, 227-246, 1998.

Jaeglé, L., D. J. Jacob, W. H. Brune, J. Faloona, D. Tan, B. G. Heikes, Y. Kondo, G. W. Sachse, B. Anderson, G. L. Gregoy, H. B. Singh, R. Pueschel, G. Ferry, D. R. Blake, and R. E. Shetter, Photochemistry of HO_x in the upper troposphere at northern midlatitudes, *J. Geophys. Res.*, *105*, 3877-3892, 2000.

Jefferson, A., D. J. Tanner, F. L. Eisele, D. D. Davis, G. Chen, J. Crawford, J. W. Huey, A. L. Torres, and H. Berresheim, OH photochemistry and methane sulfonic acid formation in the coastal Antarctic boundary layer, *J. Geophys. Res.*, *103*, 1647-1656, 1998.

Mather, J. H., P. S. Stevens, and W. H. Brune, OH and HO_2 measurements using laser-induced fluorescence, *J. Geophys. Res.*, *102*, 6427-6436, 1997.

Mauldin, R. L. III, S. Madronich, S. J. Flocke, F. L. Eisele, G. J. Frost, and A.S.H. Prevot, New insights on OH: Measurements around and in clouds, *Geophys. Res. Lett.*, *24*, 3033-3036, 1997.

Mauldin, R. L. III, G. J. Frost, G. Chen, D. J. Tanner, A.S.H. Prevot, D. D. Davis, and F. L. Eisele, OH measurements during the first aerosol characterization experiment (ACE 1): Observations and model comparisons, *J. Geophys. Res.*, *103*, 16,713-16,729, 1998.

Mauldin, R. L. III, D. J. Tanner, and F. L. Eisele, Measurements of OH during PEM-Tropics, *J. Geophys. Res.*, *104*, 5817-5827, 1999.

Mount, G. H., and F. L. Eisele, An intercomparison of tropospheric OH measurements at Fritz Peak Observatory, Colorado, *Science*, *256*, 1187-1190, 1992.

Mount, G. H., F. L. Eisele, D. J. Tanner, J. W. Brault, P. V. Johnston, J. W. Harder, E. J. Williams, A. Fried, and R. Shetter, An intercomparison of spectroscopic laser long-path and ion-assisted in situ measurements of hydroxyl concentrations during the tropospheric OH photochemistry experiment, Fall 1993, *J. Geophys. Res.*, *102*, 6437-6455, 1997.

Stevens, P. S., J. H. Mather, and W. H. Brune, Measurement of OH and HO_2 by laser-induced fluorescence at low pressure, *J. Geophys. Res.*, *99*, 3543-3557, 1994.

Stevens, P. S., *et al.*, HO_2/OH and RO_2/HO_2 ratios during the tropospheric OH photochemistry experiment: Measurement and theory, *J. Geophys. Res.*, *102*, 6379-6391, 1997.

Tan, D., I. Faloona, W. Brune, A. Weinheimer, T. Campos, B. Ridley, S. Vay, J. Collins, G. Sachse, In-situ measurements of HO_x in aircraft exhaust plumes and contrails during SUCCESS, *Geophys. Res. Lett.*, *25*, 1721-1724, 1998.

Tanner, D. J., and F. L. Eisele, Present OH measurement limits and associated uncertainties, *J. Geophys. Res.*, *100*, 2883-2892, 1995.

Tanner, D. J., A. Jefferson, and F. L. Eisele, Selected ion chemical ionization mass spectrometric measurement of OH, *J. Geophys. Res.*, *102*, 6415-6525, 1997.

Figure Captions

Figure 1. OH concentrations measured by the P-3B on flight 6 and the DC-8 on flight 8 as a function of time. The large differences in concentration are mainly due to differences in *J* values and NO. The OH concentrations shown are 60 second averages.

Figure 2. OH concentrations measured by the P-3B on three legs of flight 14 and one leg of the DC-8 flight 16 plotted as a function of time. The OH concentrations shown are 60 second averages.

Figure 3. The ratio of noontime equivalent OH measured by the DC-8 divided by that measured on the P-3B over the P-3B altitude range.

Table Captions

Table 1. Comparison of average measurements on P3-B flight and DC-8 flight 8 during flight legs in a similar location.

Table 2. Comparison of average measurements on several legs P3-B flight 14 and the only leg DC-8 flight 16 in a similar location.

Table 1

	P3-B Flight 6		DC-8 Flight 8	
	Average	Std. Dev.	Average	Std. Dev.
J-Day	74		74	
Time GMT	00:33:00		01:43:00	
Time LST	14:12:16		15:23:49	
Latitude	1.431	0.2212	1.805	0.1886
Longitude	204.816	0.2085	205.202	0.5088
Altitude (km)	0.313	0.002	0.333	0.016
$[O_3]$ (ppbv)	5.45	1.16	5.16	1.33
[CO] (ppbv)	75.1	1.31	69.0961	0.9375
[NO] (pptv)	12.2	8.45	3.04	3.44
Dew Point (K)	294.4	0.134	293.1	0.187
$[CH_2O]$ (pptv)			203	45.7
$[H_2O_2]$ (pptv)	669	22.1	791	27.4
J $O(^1D)$ sec^{-1}	5.04×10^{-5}	2.33×10^{-6}	2.34×10^{-5}	7.08×10^{-7}
J NO_2 sec^{-1}	8.84×10^{-3}	1.08×10^{-4}	7.17×10^{-3}	5.88×10^{-5}
[OH]meas (# cm^{-3})	4.69×10^{6}	2.03×10^{6}	1.64×10^{6}	9.09×10^{5}
[OH]pss (# cm^{-3})	3.58×10^{6}	1.09×10^{6}	1.25×10^{6}	4.82×10^{5}
[OH]meas/[OH]pss	1.31		1.31	
$[NO_2]$ (pptv)	11.0	9.73	11.7	8.48

* Average of $[O_3]$ from Brian Ridley and Gerry Gregory

Table 2

	P-3B Flight 14 21:55-22:06		P-3B Flight 14 00:10-00:29		P-3B Flight 14 01:37-01:57		DC-8 Flight 16 23:43-23:53	
	Average	Std. Dev.	Average	Std. Dev.	Average	Std. Dev.	Average	Std. Dev.
J-Day	94		94		94		94	
Time GMT	22:00:30		00:19:30		01:47:00		23:48:00	
Time LST	12.0136		14.3286		15.7861		13.8001	
Latitude	-21.090	0.3068	-21.026	0.2515	-20.960	0.2762	-20.9804	0.3516
Longitude	210.078	0.0021	210.052	0.0353	210.041	0.0450	210.002	0.0000
Altitude (km)	5.49	0.004	5.46	0.001	5.46	0.009	5.47	0.000
$[O_3]$ (ppbv)*	23.8	1.31	23.2		21.1	1.40	22.1	2.53
[CO] (ppbv)	46.5	2.01	46.4	1.35	45.8	1.09	41.8	1.35
[NO] (pptv)	10.5	1.42	8.49	1.72	9.27	1.73	4.71	0.501
Dew Point (K)	248.1	3.285	247.9	4.261	248.1	4.658	247.7	5.172
$[CH_2O]$ (pptv)			94.0	10.8	51.0		110	41.5
$[H_2O_2]$ (pptv)	432	0.00	560	134	654	24.6	407	72.5
J $O(^1D)$ sec^{-1}	6.99×10^{-5}	2.40×10^{-6}	4.79×10^{-5}	2.59×10^{-6}	1.95×10^{-6}	2.24×10^{-6}	4.96×10^{-5}	2.31×10^{-6}
J NO_2 sec^{-1}	1.19×10^{-2}	5.45×10^{-4}	1.11×10^{-2}	5.59×10^{-4}	9.40×10^{-3}	4.66×10^{-4}	9.95×10^{-3}	3.44×10^{-4}
[OH]meas (# cm^{-3})	2.29×10^{6}	4.66×10^{5}	1.51×10^{6}	2.35×10^{5}	1.12×10^{6}	1.75×10^{5}	2.25×10^{6}	4.95×10^{5}
[OH]pss (# cm^{-3})	3.36×10^{6}	3.40×10^{5}	2.54×10^{6}	2.46×10^{5}	1.70×10^{6}	1.12×10^{5}	2.14×10^{6}	3.50×10^{5}
[OH]meas/[OH]pss	0.68		0.59		0.66		1.05	
$[NO_2]$ (pptv)	n/a		n/a		n/a		2.90	0.432

* Average of $[O_3]$ from Brian Ridley and Gerry Gregory

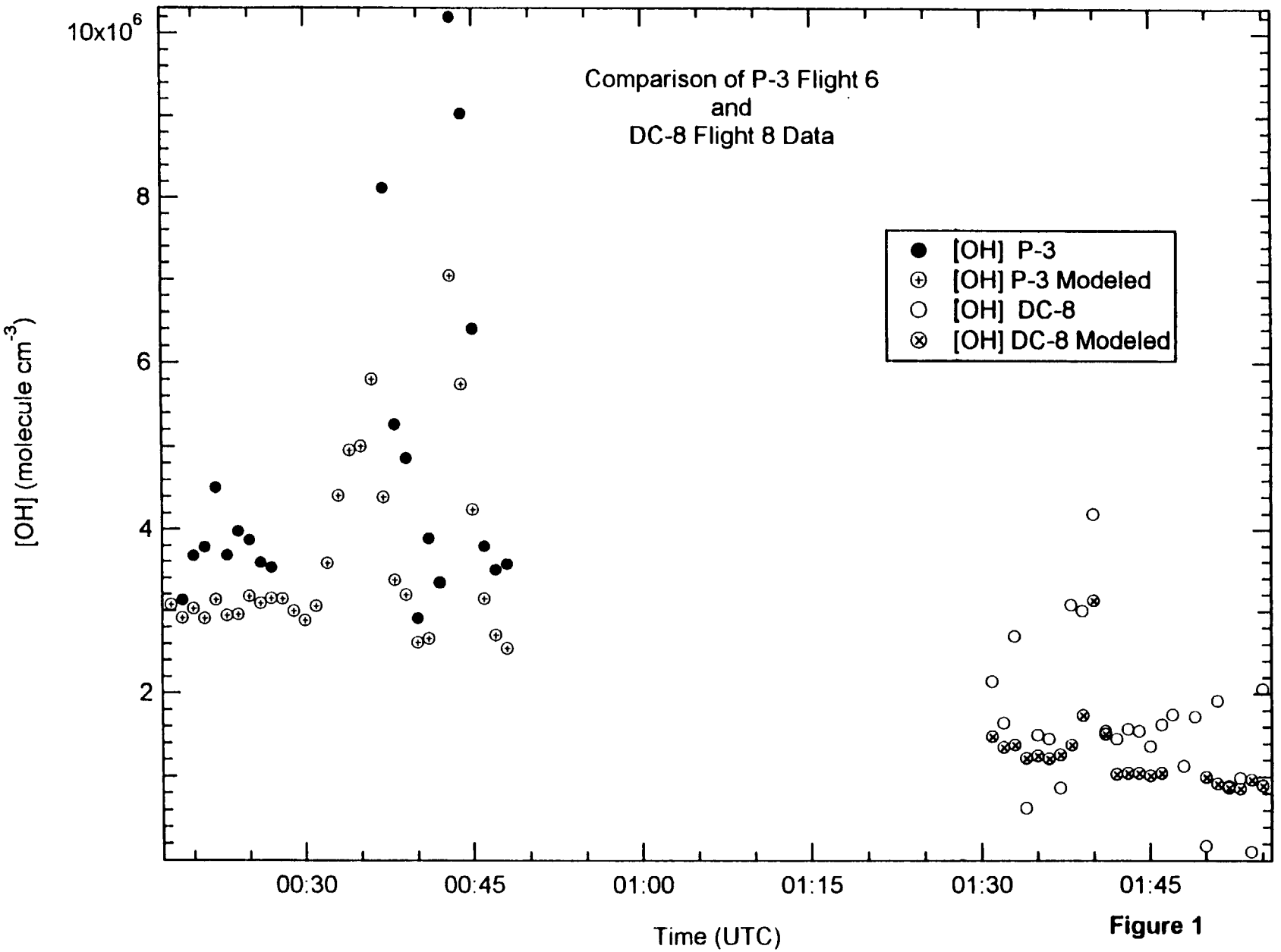
Comparison of P-3 Flight 6
and
DC-8 Flight 8 Data
[OH] P-3
[OH] P-3 Modeled
[OH] DC-8
[OH] DC-8 Modeled
10x10^6
8
6
4
2
[OH] (molecule cm^-3)
00:30
00:45
01:00
01:15
01:30
01:45
Time (UTC)

Figure 1

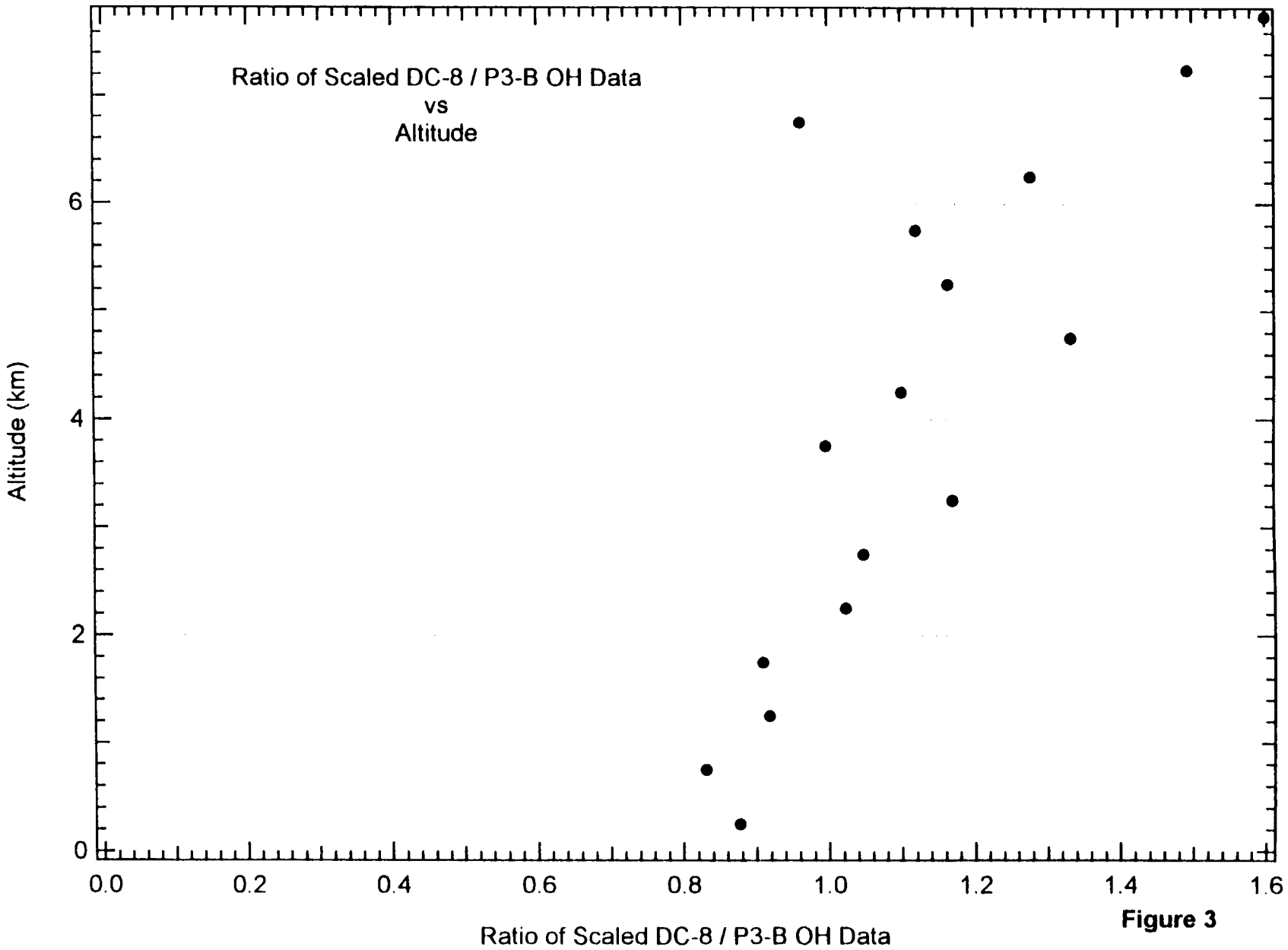
Ratio of Scaled DC-8 / P3-B OH Data
vs
Altitude
Altitude (km)
0
2
4
6
0.0
0.2
0.4
0.6
0.8
1.0
1.2
1.4
1.6
Ratio of Scaled DC-8 / P3-B OH Data

Figure 3

APPENDIX E

Chemical Ionization Mass Spectrometry Technique for the Detection of Dimethylsufoxide and Ammonia

J.B. Nowak[1], L.G. Huey[1], F.L. Eisele[1,2], D.J. Tanner[2,1], R.L. Mauldin III[2], C. Cantrell[2], E. Kosciuch[2], and D.D. Davis[1]

[1]School of Earth and Atmospheric Sciences, Georgia Institute of Technology, Atlanta, GA, 30332, USA
[2]Atmospheric Chemistry Division, National Center of Atmospheric Research, Boulder, CO, 80303, USA

Abstract- A chemical ionization mass spectrometer (CIMS) was used to study reactions of protonated ethanol clusters $(C_2H_5OH)_nH^+$ with dimethylsulfoxide (DMSO), dimethylsulfone ($DMSO_2$), ammonia (NH_3), and a series of nonmethane hydrocarbons (NMHCs) and volatile organic compounds (VOCs). The reactivity of the $(C_2H_5OH)_nH^+$ cluster ions is found to be a function of cluster size with reactivity decreasing as cluster size increases. Ethanol cluster ion distributions formed from 24 ppbv, 900 ppmv, and 1 % ethanol/N_2 gas mixtures were studied. Small $(C_2H_5OH)_nH^+$ clusters, those formed using the 24 ppbv ethanol/N_2 mixture, react at or near the collisional rate with DMSO, NH_3, acetone, and MVK. The effective ion molecule rate coefficients are: 1.8×10^{-9}, 1.5×10^{-9}, 1.0×10^{-9}, and 1.6×10^{-9} cm^3 $molec^{-1}$ s^{-1}, respectively. Only DMSO and NH_3 react with the two larger $(C_2H_5OH)_nH^+$ cluster ion distributions studied. The effective rate coefficients for DMSO and NH_3 with the 900 ppmv ethanol cluster ion distribution are 1.5×10^{-9} and 0.7×10^{-9} cm^3 $molec^{-1}$ s^{-1}, respectively. The effective rate coefficient for DMSO with the 1% ethanol/N_2 mixture is 0.35×10^{-9} cm^3 $molec^{-1}$ s^{-1}, while NH_3 reaches an equilibrium with this cluster ion distribution. Experiments show that large

$(C_2H_5OH)_nH^+$ ion clusters must be used at relative humidities greater than 50 % at 20 °C to prevent formation of and subsequent interferences from H_3O^+ ions. These results demonstrate that the $(C_2H_5OH)_nH^+$ ion chemistry can selectively detect DMSO and NH_3 under most ambient conditions with high sensitivity.

1. 0 Introduction

Chemical Ionization Mass Spectrometry (CIMS) has been used to selectively measure many atmospheric trace gases with high sensitivity. The list of species includes: the hydroxyl radical (OH), sulfuric acid (H_2SO_4), methane sulfonic acid (MSA), and nitric acid (HNO_3) [*Eisele and Tanner*, 1991; *Huey et al.*, 1998; *Mauldin et al.*, 1998; *Viggiano*, 1993]. One important feature of the CIMS method is its ability to perform measurements on fast time scales (i.e., 1 sec). For many trace gases fast time resolution measurements are essential for testing our understanding of sources and sinks. One such species falling into the above category is dimethylsulfoxide (DMSO).

DMSO is believed to be one of the major products of the OH-initiated oxidation of DMS [*Arsene et al.*, 1999; *Davis et al.*, 1999; *Davis et al.*, 1998; *Turnipseed et al.*, 1996].

$$OH + DMS \dashrightarrow SO_2, MSA, DMSO, DMSO_2, \text{other products} \quad (1)$$

DMS is a by-product of marine phytoplankton metabolic activity and its release from the ocean surface accounts for the largest fraction of biogenic gas phase sulfur emissions [*Bates et al.*, 1992; *Berresheim et al.*, 1995]. It has been hypothesized that the formation of sulfate aerosols from DMS oxidation products may significantly influence the Earth's radiation budget and possibly regulate climate [*Charlson et al.*, 1987]. DMS oxidation occurs by a complex mechanism with multiple steps that are currently the focus of many laboratory and field investigations [*Davis et al.*, 1999; *Yin et al.*, 1990]. Critical to assessing the affect of DMS oxidation on climate is understanding the chemical and physical processes that control the fate of these products in the atmosphere.

In the atmosphere DMSO reacts rapidly with OH

DMSO + OH ---- products (2)

There is, however, considerable debate as to the products of reaction 2 under atmospheric conditions. *Barnes et al.* [1989] and *Sorensen et al.* [1996] suggest that reaction 2 produces SO_2 and $DMSO_2$, though they disagree as to the yield of each product, while *Urbanski et al.* [1998] suggest that MSIA is a significant product. Though there is disagreement on the product yields of reaction 2, all the studies agree that reaction 2 leads to a DMSO photochemical lifetime of less than one hour for typical midday marine boundary layer OH levels. Another loss process for atmospheric DMSO is scavenging by cloud droplets or sea salt aerosol [*Davis et al.*, 1999; *Davis et al.*, 1998; *Debruyn et al.*, 1995]. Therefore, depending on aerosol loading, the overall lifetime of DMSO in the marine boundary layer can be even shorter than that due to photochemistry alone. The short photochemical lifetime highlights the need for fast time resolution measurements of DMSO in order to gain a comprehensive understanding of DMS oxidation.

There are few measurements of gas phase DMSO reported in the literature. The techniques utilized include: gas chromatography, gas chromatography/mass spectrometry, and a Cofer mist chamber [*Bandy et al.*, 1996; *Harvey and Lang*, 1986; *Sciare and Mihalopoulos*, 2000]. One common characteristic of all of these methods is a sampling resolution of 30 minutes or longer. Under these conditions a detailed study of DMS oxidation becomes quite difficult.

[*Berresheim et al.*, 1993] developed a CIMS method to measure DMSO on a sub-minute time scale using NH_4^+ core reagent ions. NH_3 has a proton affinity (PA) (204 kcal/mol) higher than water (166 kcal/mol) and lower than DMSO (211 kcal/mol) [*Hunter and Lias*, 2000]. Therefore, NH_4^+ ions proton transfer with DMSO in ambient air to form $DMSOH^+$. The estimated limit of detection for a 60 s integration period has been reported at 0.5 pptv. A

limitation of this technique, however, is the inability to measure NH_3.

NH_3 is an another important atmospheric trace gas for which there are few fast time response methods available. The measurement techniques include: photofragmentation/laser-induced fluorescence, denuder sampling/chemiluminescence detection, denuder sampling/ion chromatography, and filter pack sampling/colorimetric analysis [*Williams et al.*, 1992]. Recent laboratory and field measurements have led to the hypothesis that ammonia is potentially important in moderating particle nucleation and growth [*Coffman and Hegg*, 1995; *Weber et al.*, 1998]. The primary goal of this work has been to find an appropriate reagent ion for detecting both DMSO and NH_3 using the same technique. One possibility explored here is protonated ethanol, $(C_2H_5OH)H^+$.

Ethanol has a proton affinity (185.6 kcal/mol) higher than water and lower than both DMSO and NH_3 [*Hunter and Lias*, 2000]. However, $(C_2H_5OH)H^+$ efficiently clusters with any available ethanol to form an equilibrium distribution of protonated ethanol cluster ions, $(C_2H_5OH)_nH^+$, where the range of n depends on temperature and the concentration of C_2H_5OH. However, the reactivity of $(C_2H_5OH)_nH^+$ is most likely quite from that of $(C_2H_5OH)H^+$, e.g., dependant on, n, the cluster size [*Feng and Lifshitz*, 1995].

As a starting point in developing a CIMS method for detecting both DMSO and NH_3, the effective rate coefficients for reactions of $(C_2H_5OH)_nH^+$ with DMSO, NH_3, $DMSO_2$, DMS, a series of non-methane hydrocarbons (NMHCs), and a series of volatile organic compounds (VOCs) were measured (see Tables 1 and 2). The sensitivity of this ion chemistry for the detection of DMSO and NH_3 and the possibility of artifact DMSO production from ambient DMS oxidation within the instrument were also examined. Finally, a new ion-molecule reactor,

specifically designed for aircraft applications, was characterized and then used to measure DMSO in ambient air on the NASA P-3B as part of the PEM-Tropics B field program.

2.0 Experimental

2.1 Gas Standards

Isotopically labeled C^{13} DMSO and C^{13} $DMSO_2$ permeation devices were manufactured by VICI Metronics, Inc. using 99 % pure isotopically labeled compounds from Icon Services. These devices were maintained at a constant temperature and pressure. The concentrations of DMSO and $DMSO_2$ were controlled with a dynamic dilution system similar to that described by [*Goldan et al.*, 1986]. The permeation rates of each device were determined gravimetrically by the manufacturer and are traceable to NIST standards. The combined uncertainty of the C^{13} DMSO permeation tube and dilution system is estimated at ± 50% and primarily reflects the uncertainty associated with the emission rate of the permeation tubes. The combined uncertainty of the C^{13} $DMSO_2$ permeation tube and dilution is estimated at ± a factor of 5 and reflects additional difficulties associated with that particular permeation device.

NH_3 concentrations were determined by monitoring the absorption of the 185 nm mercury atomic line. An NH_3 absorption cross section at 185 nm of 4.3×10^{-18} cm^2 $molecule^{-1}$ was used [*Lovejoy*, 1999]. The nonmethane hydrocarbons (NMHCs) and volatile organic compounds (VOCs) used in these experiments were obtained either from Scott Gases or Apel-Riemer Environmental, Inc. The mixing ratios of the NMHC and VOC standards were between 10 and 20 ppmv.

2.2 Ion-Molecule Reactor

The CIMS apparatus consists of two sections, an ion-molecule reactor where the

sampling and chemical ionization is performed and a vacuum system housing a quadruple mass spectrometer and an electron multiplier detector. Two mass spectrometers were used in this work. The laboratory experiments were performed on a dual channel diffusion pump system previously described by [*Eisele and Tanner*, 1993]. The ambient air measurements were performed on the top channel of the 4 channel NCAR CIMS system as described by *Mauldin et al.* [2001]. In both cases the same ion-molecule reactor was used.

The ion-molecule reactor consists of two sections, the transverse ion source, conceptually similar to that described by *Eisele and Hanson* [2000], and the transport tube, as shown in figure 1. The ion source is a 7 cm x 8 cm x 2.5 cm teflon block with a 1.9 cm diameter hole machined through the center. A 9 cm long by 1.9 cm inner diameter teflon tube fits snugly into the teflon block mating with the center hole to form the sampling inlet. Ambient air or dry N_2 is sampled through the inlet at 4 SLPM. A radioactive ion source, ^{241}Am, and the transport tube are located on opposite sides of the sampling tube. Between the radioactive source and transport tube is the ion-molecule reaction region (see Figure 1). The stainless steel transport tube is 22.86 cm long with a diameter of 0.762 cm and has a 0.025 cm diameter orifice located at its top. A buffer gas of dry N_2 is continuously flowed in front of the orifice to minimize any ambient air or un-ionized reagent gas from entering the transport tube.

The two advantages of using this type of ion-molecule reactor on an aircraft platform are: 1) that the transport tube provides a convenient way to extend the sampling inlet outside of an airplane's boundary layer; and 2) contact between the inlet wall and the ambient air sample is minimized by aligning the sampling tube with the ambient air flow, thus, allowing for straight path sampling into the reaction region. Minimal wall interactions should also increase

instrument response time by inhibiting reversible desorption from the walls.

2.3 Reaction Time

The protonated ethanol cluster ions are produced by flowing 1 SLPM of an ethanol/N2 mixture over an ^{241}Am radioactive ion source. ^{241}Am releases α particles that form $(C_2H_5OH)H^+$ through a series of reactions. These ions rapidly cluster with ethanol to form an equilibrium distribution of $(C_2H_5OH)_nH^+$. The $(C_2H_5OH)_nH^+$ ions are accelerated across the reaction region through the path of the ambient sample by an electrical field. The electric field is produced by applying a potential of 1.6 kV to the radioactive ion source and 100 V to the transport tube.

The drift time (i.e., reaction time) of the ions across the reaction region can be calculated as

$$t_d = \frac{L^2}{kV} \qquad (3)$$

where L is the length of the reaction region, V is the electrical potential across the region, and k is the mobility of the ion. However, there are two difficulties to applying equation (3) to the set-up used here. First, k is unknown because the ethanol cluster size distribution in the reaction region is impossible to predict due to a lack of thermodynamic parameters. Second, this formula determines the drift time for ions between two infinitely long parallel plates and does not take into account the specific geometries of the ion-molecule reactor or any dielectric effects from the teflon housing to the electric field. Therefore, an independent determination of the reaction time was obtained using SF_6^- as the reagent ion and adding a SO_2/N_2 mixture to the ion-molecule reactor to estimate the effective electric field strength.

The rate constant for the $SF_6^- + SO_2$ reaction has been well established as 1.0×10^{-9} cm^3

molecs^{-1} s^{-1}, independent of temperature and pressure [*Arnold et al.*, 2000; *Ferguson*, 1976; *Huey et al.*, 1995; *Streit*, 1982]. The reaction time was calculated from measuring the decay of SF_6^- as a function of the SO_2 concentration. From these experiments a reaction time of 7 ms was obtained. Using this reaction time, the reaction region length (L = 1.9 cm), and 1.90 $cm^2V^{-1}s^{-1}$ as the SF_6^- ion mobility [*Lakdawala and Moruzzi*, 1980], the effective electric field strength (V_{eff}) is calculated to be 270 V.

The largest uncertainty with estimating the reaction time lies in the calculation of the ion mobility of the ethanol cluster ion distribution. The relationship between ion mobility and mass has been difficult to quantify (e.g., [*Bohringer et al.*, 1987; *Tammet*, 1995]). Along with mass, ion structure is known to affect mobility [*Kim and Spangler*, 1985]. Again, since the protonated ethanol cluster size distribution is unknown, it is even more difficult to relate mass and ion structure to mobility of the ethanol cluster ion distribution. *Makela et al.* [1996] measured the mobility of acetone cluster ions produced in a manner similar to the ethanol cluster ions in this study (i.e., flowing 1000 ppmv of acetone over a radioactive ion source) at 1.3 - 1.5 $cm^2\ V^{-1}\ s^{-1}$. Since the mass of acetone is similar to that of ethanol (58 amu to 46 amu), it is reasonable to assume that the ion mobility of the protonated ethanol cluster ions in this study is similar. Furthermore, data from *Kilpatrick* [1971] suggests that the ion mobility only changes approximately by a factor of 2 for an order of magnitude change in mass. Therefore, using 1.4 $cm^2\ V^{-1}\ s^{-1}$, the middle of the range from the acetone cluster study, as the ion mobility, the reaction time is estimated from equation (3) at 10 ms. Given the results of *Kilpatrick* [1971], this estimate is probably good within a factor of 2. Based alone on the mass difference between acetone and ethanol, the uncertainty in the reaction time is estimated at ± 20 - 30 %.

2.3 Transport Tube Effects

Since water from the ambient sample and ethanol from the reagent gas are prevented from entering the transport tube by the use of N_2 as a buffer gas in front of the transport tube orifice, the distribution of $(C_2H_5OH)_nH^+$ cluster ions in the transport tube is dramatically altered from that in the reaction region. Weakly bound cluster ions dissociate in the transport tube allowing the $(C_2H_5OH)_nH^+$ ions to reach a new equilibrium distribution. The minimum cluster bond strength needed to transverse the transport tube has been estimated here for a neutral, x, and an ion, y^+, reacting to form an equilibrium cluster xy^+

$$x + y^+ \underset{k_r}{\overset{k_f}{\rightleftharpoons}} xy^+ \qquad (4)$$

In this set-up, with the pressure in the transport tube at approximately 50 torr and a ~500 sccm mass flow through the transport tube, the resulting residence time is approximately 50 ms. From this residence time, the largest allowable k_r is 20 s^{-1}. If k_f is assumed to be greater than 10^{-10} s^{-1}, K_{eq} equals 5×10^{-12}. Under room temperature conditions and using 6-7 kcal/mol as a reasonable assumption for $T\Delta S$, solving for ΔH gives a minimum ΔH_{rxn} to traverse the transport tube of 20-21 kcal/mol. Thus, the transport tube greatly affects what is detected since clusters with a bond energy of less than 20-21 kcal/mol will dissociate in the transport tube before being detected. As a result, the transport tube makes the observed mass spectrum less complicated and easier to interpret.

Unfortunately, due to the transport tube set-up used in this work, it is impossible to know the detailed size distribution of ethanol clusters in the reaction region. However, it is known that the observed ethanol cluster distribution is quite different from that in the reaction region.

Because of this, in order to qualitatively test for reactivity as a function of cluster size, experiments were performed using ethanol/N_2 reagent gas mixtures of 24 ppbv, 900 ppmv, and 1% C_2H_5OH to produce the reagent ions. In all cases, the dominant $(C_2H_5OH)_nH^+$ clusters observed in the mass spectra were the monomer, $(C_2H_5OH)H^+$, the dimer, $(C_2H_5OH)_2H^+$, and the trimer, $(C_2H_5OH)_3H^+$. Since the ΔH_{rxn} of

$$(C_2H_5OH)_2H^+ + C_2H_5OH \rightarrow (C_2H_5OH)_3H^+ \qquad (5)$$

has been reported as -21.4 kcal/mol [*Feng and Lifshitz*, 1995], it is not surprising that no evidence of $(C_2H_5OH)_4H^+$ or larger is seen in the mass spectra (i.e., the larger clusters dissociate in the transport tube before detection). Under the 24 ppbv ethanol conditions, the monomer and dimer were predominantly observed. At the higher ethanol levels, the monomer and dimer signals were seen increasing and the trimer was also observed. These results suggest that there are more large ethanol clusters in the reaction region under the higher ethanol conditions than under the 24 ppbv ethanol conditions.

3.0 Results

3.1 Effective Rate Coefficients

Effective rate coefficients were determined for the ion molecule reaction of $(C_2H_5OH)_nH^+$ with DMSO, NH_3, CH_4, DMS, and select NMHCs and VOCs using 24 ppbv, 900 ppmv, and 1% ethanol/N_2 reagent gas mixtures. The effective rate coefficients were determined by monitoring the depletion of the total ethanol signal (i.e., the sum of the monomer, dimer, and trimer signals) as a function of the neutral reactant added to a dry N_2 sample flow. Given the combined uncertainties in the estimated reaction time and the gas standard dilutions, the uncertainty in the effective ion-molecule rate coefficients reported here is estimated at a factor of 2.

The measured effective rate coefficients for the ion molecule reactions of $(C_2H_5OH)_nH^+$ are reported in Tables 1 and 2 along with the proton affinities of the neutral reactants. Listed in Table 2 are all species tested that react with $(C_2H_5OH)_nH^+$ at $< 5 \times 10^{-12}$ cm^3 molec^{-1} s^{-1} under all ethanol conditions. Calculated collision rate coefficients, determined by the method of *Su and Chesnavich* [1982], in the limit that the ethanol cluster size approaches infinity, are reported for selected reactions. As shown in Table 1, DMSO, NH_3, acetone, and methyl vinyl ketone (MVK) react with small protonated ethanol clusters (i.e., 24 ppbv ethanol/N_2 reagent gas mixture) at or near the calculated collision rate. The effective rate coefficients are: 1.8×10^{-9}, 1.5×10^{-9}, 1.0×10^{-9}, and 1.6×10^{-9} cm^3 molec^{-1} s^{-1}, respectively. $DMSO_2$ was also found to react with small protonated ethanol clusters at or near the gas kinetic rate, however, the additional uncertainty in the $DMSO_2$ standard has prevented a more precise determination to be made. Only DMSO and NH_3 react with the larger ethanol cluster ion distribution (i.e., 900 ppmv ethanol/N_2 reagent gas mixture) with effective rate coefficients of 1.5×10^{-9} and 0.7×10^{-9} cm^3 molec^{-1} s^{-1}. DMSO and NH_3 are also the only species to react with the largest ethanol cluster ion distribution (i.e,1% ethanol/N_2 reagent gas mixture), however, the DMSO effective ion molecule rate has slowed to 0.35×10^{-9} cm^3 molec^{-1} s^{-1}, while only a lower limit on the NH_3 reaction can be given because the system equilibrates.

$$(C_2H_5OH)_nH^+ + NH_3 \rightarrow (NH_3)(C_2H_5OH)_lH^+ + nC_2H_5OH \quad (6)$$

The ratio of product ions to reactant ions, $\frac{(NH_3)(C_2H_5OH)_lH^+}{(C_2H_5OH)_nH^+}$, is temperature and ethanol concentration dependant. In the laboratory at 21° C and 1% ethanol/N_2 reagent gas mixture this ratio is 2.5×10^{-12}. These experiments clearly show that the reactivity of the $(C_2H_5OH)_nH^+$ ions

is a function of cluster size.

3.2 Relative Humidity Tests

The $(C_2H_5OH)_nH^+$ ion distribution was studied as a function of relative humidity (RH). At low ethanol concentrations (i.e., 24 ppbv ethanol) the $(C_2H_5OH)_nH^+$ ions are converted to the water clusters $(H_2O)_2H^+$ (37 amu) and $(H_2O)_3H^+$ (55 amu) for RH > 50%. But for the same RH under the 900 ppmv and 1% ethanol conditions, the dominant peaks are the ethanol monomer, dimer, and trimer. At RH < 25 % the ethanol ion peaks dominate independent of ethanol concentration. Thus, these experiments suggest that when the RH > 50 % it is necessary to use a reagent gas mixture with greater than 900 ppmv of ethanol to preserve the $(C_2H_5OH)_nH^+$ chemistry. It is important to maintain the $(C_2H_5OH)_nH^+$ chemistry because $(H_2O)_mH^+$ is more reactive than $(C_2H_5OH)_nH^+$ and shifting the ion chemistry to $(H_2O)_mH^+$ would decrease the selectivity of this technique.

Additional experiments were performed to examine the effect of H_2O on the effective ion molecule rate constant for DMSO and NH_3. This was done with a 900 ppmv ethanol/N_2 ethanol reagent gas mixture by adding a constant amount of DMSO, 70 pptv, or NH_3, 400 pptv, while humidifying the UHP zero air sample stream from 0 to 85% relative humidity. Under these conditions less than 20% of the total ethanol signal was converted to water clusters, thereby, preserving the $(C_2H_5OH)_nH^+$ chemistry. The effective ion molecule rate coefficients for DMSO and NH_3 changed by less then 20% from 0 to 80 % RH.

3.3 DMS Interferences

The species benzene (C_6H_6) and methanol (CH_3OH) could give ion products ($C_6H_6H^+$ or

$CH_3OH{\cdot}C_2H_5OHH^+$) that have the same mass as $DMSOH^+$. However, since neither C_6H_6 or CH_3OH were observed to react with $(C_2H_5OH)_nH^+$, they can not be considered as significant interferences in the detection of DMSO. Recalling that DMSO is produced by the oxidation of DMS, a potential interference is artifact DMSO production by ion molecule processes from ambient DMS present in the reaction region. To test for this possibility, DMS was added to a UHP zero air sample flow in concentrations ranging from 600 pptv to 69 ppbv under the following conditions: low humidity, high humidity, low humidity with 200 ppbv O_3, and high humidity with 200 ppbv O_3. The results showed that DMS did not react with $(C_2H_5OH)_nH^+$ under any of the above conditions to produce a product at the mass of $DMSH^+$, $DMSOH^+$, or C^{13} $DMSOH^+$.

3.4 Ambient Air Tests

The protonated ethanol ion chemistry was used to measure DMSO on one channel of the NCAR four channel CIMS system deployed on the NASA P-3B aircraft during the GTE-PEM Tropics B field program in March/April of 1999. To maximize the selectivity during these measurements a 1 % ethanol reagent gas mixture was used. The sensitivity of the instrument to DMSO was measured to be 1 count per second (Hz) per pptv of DMSO at a total ethanol signal of 10 kHz relative to the calibration C^{13} DMSO. This agrees quite well with the sensitivity of 0.9 Hz estimated from the experimentally determined effective rate coefficient under the 1 % ethanol conditions. The background signal at the DMSO product ion mass was found to be no greater than 1 Hz (i.e., 1 pptv) which gives a limit of detection for DMSO of 0.50 pptv for a 60 s integration period. As expected, the DMSO sensitivity was not affected by ambient relative

humidity under high ethanol conditions to within ± 20 %.

Figure 2 compares a mass spectrum taken in the boundary layer at 75% RH during flight 16 of PEM-Tropics B, panel A, with one taken in the laboratory at 80 % RH, panel B. Note that the ion signal axis is linear from 0 - 1000 Hz and logarithmic above 1000 Hz. The discrepancy in total ion signal between the two spectra is primarily a result of the difference in pumping speeds between the field and laboratory instruments. As seen in figure 2, the ethanol cluster peaks dominate both spectra indicating the preservation of the $(C_2H_5OH)_nH^+$ ion chemistry under these high RH conditions. Also seen in panel B are NH_4^+ and $(C_2H_5OH)H^+NH_4^+$ due to NH_3 contamination in the deionized water used to adjust the relative humidity.

Figure 3 presents a time series plot of DMSO taken during the midday boundary and buffer layer sampling runs during flight 16 pf PEM-Tropics B. The data shown here were recorded at 15 second time resolution. This time series highlights the response time of the technique. Here one can easily see the sharp change in DMSO levels when switching between the boundary and buffer layers. This suggests that the response time of this technique is faster than 15 seconds making it highly suitable for aircraft studies. The data also show significant levels of DMSO in both the boundary and buffer layers. As expected, boundary layer DMSO levels were 2-3 times greater than those observed in the buffer layer. A more detailed comparison of these observations with model simulations is presented by *Nowak et al.* [2001].

4.0 Summary and Discussion

Overall, the protonated ethanol cluster ion chemistry presented in this work appears to be a highly selective and sensitive method for detecting certain atmospheric trace gases. However,

controlling cluster size is critical for utilizing this ion chemistry in field studies. As shown in Table 2, many species with PA > C_2H_5OH do not react with any size $(C_2H_5OH)_nH^+$ clusters. As indicated by Table 1, for species that do react the effective ion molecule rate coefficient decreases with increasing cluster size. Not only does cluster size influence the effective ion molecule rate coefficient, cluster size also establishes the ambient conditions under which the ion chemistry will be effective. As discussed in Section 3.2, at high levels of water vapor small $(C_2H_5OH)_nH^+$ clusters are transformed into $(H_2O)_mH^+$ via

$$(C_2H_5OH)_nH^+ + mH_2O \rightarrow (H_2O)_mH^+ + nC_2H_5OH. \quad (7)$$

At high relative humidity a minimum cluster size is needed to preserve the $(C_2H_5OH)_nH^+$ ion chemistry and the selectivity of the technique. Thus, at high relative humidity a minimum cluster size is needed to preserve the $(C_2H_5OH)_nH^+$ ion chemistry. This means that the ethanol cluster ion size determines the selectivity and sensitivity for a given RH range; and so, to effectively apply the protonated ethanol cluster ion chemistry to field measurements, the ethanol cluster ion size must be matched not only to the atmospheric species of interest but also to the ambient conditions.

Of the species examined in this study the $(C_2H_5OH)_nH^+$ ion chemistry is best suited for the detection of DMSO. Since DMSO is one of the few species that reacts with large $(C_2H_5OH)_nH^+$ clusters, a high level of selectivity is inherent in this ion chemistry. The use of large ethanol clusters also eliminates any sensitivity dependence on humidity seen in other CIMS techniques due to cluster ions with different numbers of water molecules reacting at different rates [*Seeley et al.*, 1997]. As demonstrated under ambient conditions during PEM-Tropics B, the combination of high selectivity, insensitivity to ambient RH levels, and fast time response

and resolution makes this technique well suited for ambient measurements of DMSO.

For many of the same reasons, this technique also shows considerable promise for the detection of NH_3. However, more attention needs to be paid to the $(C_2H_5OH)_nH^+$ cluster ion size than for DMSO. At the largest $(C_2H_5OH)_nH^+$ clusters used in this study, NH_3 reaches an equilibrium with the ethanol cluster ions which is dependent on temperature and ethanol concentrations. Consequently, the sensitivity could be strongly dependant on temperature and ethanol concentration of the reagent gas mixture. No species in this study, expect for DMSO, react with $(C_2H_5OH)_nH^+$ when using a 900 ppmv reagent gas mixture. Therefore, careful control of the $(C_2H_5OH)_nH^+$ cluster ion size distribution is critical to maintain the high selectivity while eliminating the difficulties of the equilibrium reaction. In addition, sampling and background issues need to be further addressed as highlight by the presence of NH_3 related peaks shown in figure 2 panel B.

Laboratory results also suggest that this method could be used to detect acetone and MVK under low ambient relative humidity conditions. Acetone is believed to be an upper tropospheric HO_x source and to partition reactive nitrogen into PAN [*Arnold et al.*, 1997; *Crawford et al.*, 1999; *Singh et al.*, 2000; *Singh et al.*, 1995]. The low water levels in the upper troposphere may allow for fast-time resolution acetone measurements using small protonated ethanol clusters. The OH-initiated oxidation of isoprene has been found to yield MVK, methacrolein (MACR), and formeldehyde as major products [*Paulson et al.*, 1992; *Tuazon and Atkinson*, 1990]. Since MACR does not react with small $(C_2H_5OH)_nH^+$ clusters (see Table 2), this technique could potentially be used to differentiate between MVK and MACR when studying isoprene oxidation mechanisms. However, since isoprene oxidation is of most interest

in the boundary layer, ambient relative humidity conditions are often too high for use of the small $(C_2H_5OH)_nH^+$ clusters. Further laboratory study examining the possibility of using the small $(C_2H_5OH)_nH^+$ cluster in conjunction of with a dryer to make boundary layer MVK measurements is needed.

5.0 Conclusions

The reactivity of $(C_2H_5OH)_nH^+$ cluster ions has been found to be inversely proportional to cluster size, i.e., the larger clusters react with fewer species. Only two species, DMSO and NH_3, were found to react with the large $(C_2H_5OH)_nH^+$ cluster ions. DMSO reacts at or near the collisional rate with all size ethanol clusters examined. NH_3, also, reacts with all size ethanol clusters, though, it reaches an equilibrium with the larger clusters. For ambient measurements at RH > 50%, larger $(C_2H_5OH)_nH^+$ cluster ions must be utilized. Therefore, a high level of selectivity is inherent in the $(C_2H_5OH)_nH^+$ cluster ion chemistry. Interference testing shows that DMSO is not produced from DMS by ion processes in the ion-molecule reactor. $(C_2H_5OH)_nH^+$ cluster ion chemistry has been successfully used to measure DMSO from an aircraft platform during PEM-Tropics B. Laboratory studies suggest this ion chemistry be used to detect NH_3 under ambient atmospheric conditions.

The ion-molecule reactor described here has shown to be viable for aircraft trace gas measurements. While the transport tube may limit the number of species that can be detected, due to the dissociation of weakly bound clusters, it eliminates possible interferences from those same clusters, makes the mass spectrum easier to interpret, and extends the sampling inlet outside the airplane's boundary layer.

References

Arnold, F., V. Burger, B. DrosteFanke, F. Grimm, A. Krieger, J. Schneider, and T. Stilp, Acetone in the upper troposphere and lower stratosphere: Impact on trace gases and aerosols, *Geophysical Research Letters*, *24* (23), 3017-3020, 1997.

Arnold, S.T., J.V. Seeley, J.S. Williamson, P.L. Mundis, and A.A. Viggiano, New apparatus for the study of ion-molecule reactions at very high pressure (25-700 Torr): A turbulent ion flow tube (TIFT) study of the reaction of SF6-+SO2, *Journal of Physical Chemistry A*, *104* (23), 5511-5516, 2000.

Arsene, C., I. Barnes, and K.H. Becker, FT-IR product study of the photo-oxidation of dimethyl sulfide: Temperature and O-2 partial pressure dependence, *Physical Chemistry Chemical Physics*, *1* (24), 5463-5470, 1999.

Bandy, A., D.C. Thornton, B.W. Blomquist, S. Chen, T.P. Wade, J.C. Ianni, G.M. Mitchell, and W. Nadler, Chemistry of dimethyl sulfide in the equatorial Pacific atmosphere, *Geophysical Research Letters*, *23* (7), 741-744, 1996.

Barnes, I., V. Bastian, K.H. Becker, and D. Martin, Fourier-Transform Ir Studies of the Reactions of Dimethyl- Sulfoxide with Oh, No3, and Cl Radicals, *Acs Symposium Series*, *393*, 476-488, 1989.

Bates, T.S., B.K. Lamb, A. Guenther, J. Dignon, and R.E. Stoiber, Sulfur Emissions to the Atmosphere from Natural Sources, *Journal of Atmospheric Chemistry*, *14* (1-4), 315-337, 1992.

Berresheim, H., D.J. Tanner, and F.L. Eisele, Real-Time Measurement of Dimethyl-Sulfoxide in Ambient Air, *Analytical Chemistry*, *65* (1), 84-86, 1993.

Berresheim, H., P.H. Wine, and D.D. Davis, Sulfur in the atmosphere, in *Composition, Chemistry, and Climate of the Atmosphere*, edited by H.B. Singh, pp. 527, Van Nostrand Reinhold, New York, 1995.

Bohringer, H., D.W. Fahey, W. Lindinger, F. Howorka, F.C. Fehsenfeld, and D.L. Albritton, Mobilities of Several Mass-Identified Positive and Negative- Ions in Air, *International Journal of Mass Spectrometry and Ion Processes*, *81*, 45-65, 1987.

Charlson, R.J., J.E. Lovelock, M.O. Andreae, and S.G. Warren, Oceanic Phytoplankton, Atmospheric Sulfur, Cloud Albedo and Climate, *Nature*, *326* (6114), 655-661, 1987.

Coffman, D.J., and D.A. Hegg, A Preliminary-Study of the Effect of Ammonia on Particle Nucleation in the Marine Boundary-Layer, *Journal of Geophysical Research-Atmospheres*, *100* (D4), 7147-7160, 1995.

Crawford, J., D. Davis, J. Olson, G. Chen, S. Liu, G. Gregory, J. Barrick, G. Sachse, S. Sandholm, B. Heikes, H. Singh, and D. Blake, Assessment of upper tropospheric HOx sources over the tropical Pacific based on NASA GTE/PEM data: Net effect on HOx and other photochemical parameters, *Journal of Geophysical Research-Atmospheres*, *104* (D13), 16255-16273, 1999.

Davis, D., G. Chen, A. Bandy, D. Thornton, F. Eisele, L. Mauldin, D. Tanner, D. Lenschow, H. Fuelberg, B. Huebert, J. Heath, A. Clarke, and D. Blake, Dimethyl sulfide oxidation in the equatorial Pacific: Comparison of model simulations with field observations for

DMS, SO2, H2SO4(g), MSA(g), MS, and NSS, *Journal of Geophysical Research-Atmospheres*, *104* (D5), 5765-5784, 1999.

Davis, D., G. Chen, P. Kasibhatla, A. Jefferson, D. Tanner, F. Eisele, D. Lenschow, W. Neff, and H. Berresheim, DMS oxidation in the Antarctic marine boundary layer: Comparison of model simulations and field observations of DMS, DMSO, DMSO2, H2SO4(g), MSA(g), and MSA(p), *Journal of Geophysical Research-Atmospheres*, *103* (D1), 1657-1678, 1998.

Debruyn, W.J., E. Swartz, J.H. Hu, J.A. Shorter, P. Davidovits, D.R. Worsnop, M.S. Zahniser, and C.E. Kolb, Henrys Law Solubilities and Setchenow Coefficients for Biogenic Reduced Sulfur Species Obtained from Gas-Liquid Uptake Measurements, *Journal of Geophysical Research-Atmospheres*, *100* (D4), 7245-7251, 1995.

Eisele, F.L., and D.R. Hanson, First measurement of prenucleation molecular clusters, *Journal of Physical Chemistry A*, *104* (4), 830-836, 2000.

Eisele, F.L., and D.J. Tanner, Ion-Assisted Tropospheric Oh Measurements, *Journal of Geophysical Research-Atmospheres*, *96* (D5), 9295-9308, 1991.

Eisele, F.L., and D.J. Tanner, Measurement of the Gas-Phase Concentration of H2so4 and Methane Sulfonic-Acid and Estimates of H2so4 Production and Loss in the Atmosphere, *Journal of Geophysical Research-Atmospheres*, *98* (D5), 9001-9010, 1993.

Feng, W.Y., and C. Lifshitz, The Reactivity of Neat and Mixed Proton-Bound Ethanol Clusters, *International Journal of Mass Spectrometry and Ion Processes*, *150*, 13-25, 1995.

Ferguson, E.E., Some aspects of negative ion chemistry, *International Journal of Mass Spectrometry and Ion Processes*, *19*, 53-70, 1976.

Goldan, P.D., W.C. Kuster, and A.L. Albritton, A dynamic dilution system for the production of sub-ppb concentrations of reactive and labile species, *Atmospheric Environment*, *20* (6), 1203-1209, 1986.

Harvey, G.R., and R.F. Lang, Dimethylsulfoxide and dimethylsulfone in the marine atmosphere, *Geophysical Research Letters*, *13*, 49-51, 1986.

Huey, L.G., E.J. Dunlea, E.R. Lovejoy, D.R. Hanson, R.B. Norton, F.C. Fehsenfeld, and C.J. Howard, Fast time response measurements of HNO3 in air with a chemical ionization mass spectrometer, *Journal of Geophysical Research-Atmospheres*, *103* (D3), 3355-3360, 1998.

Huey, L.G., D.R. Hanson, and C.J. Howard, Reactions of Sf6- and I- with Atmospheric Trace Gases, *Journal of Physical Chemistry*, *99* (14), 5001-5008, 1995.

Hunter, E.P., and S.G. Lias, "Proton affinity Evaluation" in NIST Chemistry WebBook,NIST STandard Reference Database Number 69, Eds. W.G. Mallard and P.J. Linstrom,National Institute of Standards and technology, Gaithersburg MD, 20899 (http://webbook.nist.gov), 2000.

Kilpatrick, F.W., An experimental mass-mobility relation for ions at atmospheric pressure, *Proceedings of Annual Conference of Mass Spectroscopy 19th*, 320, 1971.

Kim, S.H., and G.E. Spangler, Ion Mobility spectrometry/mass spectrometry (IMS/MS) of two structually different ions having identical ion mass, *Analytical Chemistry*, *57* (2), 567-569, 1985.

Lakdawala, V.K., and J.L. Moruzzi, Measurements of attachment coefficients and ionic mobilities in SF_6-nitrogen mixtures over the low-energy range 1.2 - 4.0 eV, *Journal of*

Physics D: Applied Physics, *13*, 1439-1445, 1980.

Lovejoy, E.R., Ion trap studies of H+(H2SO4)(m)(H2O)(n) reactions with water, ammonia, and a variety of organic compounds, *International Journal of Mass Spectrometry*, *191*, 231-241, 1999.

Makela, J.M., V. Jokinen, T. Mattila, A. Ukkonen, and J. Keskinen, Mobility distribution of acetone cluster ions, *Journal of Aerosol Science*, *27* (2), 175-190, 1996.

Mauldin, R.L., F.L. Eisele, D.J. Tanner, C.A. Cantrell, E. Kosciuch, J.B. Nowak, G. Chen, L. Wang, D. Davis, B.A. Ridley, and B. Lefer, Measurements of OH aboard the NASA P-3 during PEM-Tropics B, *Jounal of Geophysical Research, submitted*, 2001.

Mauldin, R.L., D.J. Tanner, and F.L. Eisele, A new chemical ionization mass spectrometer technique for the fast measurement of gas phase nitric acid in the atmosphere, *Journal of Geophysical Research-Atmospheres*, *103* (D3), 3361-3367, 1998.

Nowak, J.B., D.D. Davis, G. Chen, F.L. Eisele, R.L. Mauldin, D.J. Tanner, C. Cantrell, E. Kosciuch, A. Bandy, D. Thornton, and A. Clarke, Airborne observations of DMSO, DMS, and OH at marine tropical latitudes, *Geophysical Research Letters*, *28* (11), 2201-2204, 2001.

Paulson, S.E., R.C. Flagan, and J.H. Seinfeld, Atmospheric Photooxidation of Isoprene .1. The Hydroxyl Radical and Ground-State Atomic Oxygen Reactions, *International Journal of Chemical Kinetics*, *24* (1), 79-101, 1992.

Sciare, J., and N. Mihalopoulos, A new technique for sampling and analysis of atmospheric dimethylsulfoxide (DMSO), *Atmospheric Environment*, *34* (1), 151-156, 2000.

Seeley, J.V., R.A. Morris, and A.A. Viggiano, Rate constants for the reactions of CO3-(H2O)(n=0-5)+SO2: Implications for CIMS detection of SO2, *Geophysical Research Letters*, *24* (11), 1379-1382, 1997.

Singh, H., Y. Chen, A. Tabazadeh, Y. Fukui, I. Bey, R. Yantosca, D. Jacob, F. Arnold, K. Wohlfrom, E. Atlas, F. Flocke, D. Blake, N. Blake, B. Heikes, J. Snow, R. Talbot, G. Gregory, G. Sachse, S. Vay, and Y. Kondo, Distribution and fate of selected oxygenated organic species in the troposphere and lower stratosphere over the Atlantic, *Journal of Geophysical Research-Atmospheres*, *105* (D3), 3795-3805, 2000.

Singh, H.B., M. Kanakidou, P.J. Crutzen, and D.J. Jacob, High-Concentrations and Photochemical Fate of Oxygenated Hydrocarbons in the Global Troposphere, *Nature*, *378* (6552), 50-54, 1995.

Sorensen, S., H. FalbeHansen, M. Mangoni, J. Hjorth, and N.R. Jensen, Observation of DMSO and CH3S(O)OH from the gas phase reaction between DMS and OH, *Journal of Atmospheric Chemistry*, *24* (3), 299-315, 1996.

Streit, G.E., Negative ion chemistry and electron affinity of SF_6, *Journal of Chemical Physics*, *77*, 826-833, 1982.

Su, T., and W.J. Chesnavich, Parametrization of the ion-polar molecule collision rate constant by trajectory calculations, *Journal of Chemical Physics*, *76* (10), 5183-5185, 1982.

Tammet, H., Size and Mobility of Nanometer Particles, Clusters and Ions, *Journal of Aerosol Science*, *26* (3), 459-475, 1995.

Tuazon, E.C., and R. Atkinson, A Product Study of the Gas-Phase Reaction of Isoprene with the Oh Radical in the Presence of Nox, *International Journal of Chemical Kinetics*, *22* (12), 1221-1236, 1990.

Turnipseed, A.A., S.B. Barone, and A.R. Ravishankara, Reaction of OH with dimethyl sulfide .2. Products and mechanisms, *Journal of Physical Chemistry*, *100* (35), 14703-14713, 1996.

Urbanski, S.P., R.E. Stickel, and P.H. Wine, Mechanistic and kinetic study of the gas-phase reaction of hydroxyl radical with dimethyl sulfoxide, *Journal of Physical Chemistry A*, *102* (51), 10522-10529, 1998.

Viggiano, A.A., In-Situ Mass-Spectrometry and Ion Chemistry in the Stratosphere and Troposphere, *Mass Spectrometry Reviews*, *12* (2), 115-137, 1993.

Weber, R.J., P.H. McMurry, L. Mauldin, D.J. Tanner, F.L. Eisele, F.J. Brechtel, S.M. Kreidenweis, G.L. Kok, R.D. Schillawski, and D. Baumgardner, A study of new particle formation and growth involving biogenic and trace gas species measured during ACE 1, *Journal of Geophysical Research-Atmospheres*, *103* (D13), 16385-16396, 1998.

Williams, E.J., S.T. Sandholm, J.D. Bradshaw, J.S. Schendel, A.O. Langford, P.K. Quinn, P.J. Lebel, S.A. Vay, P.D. Roberts, R.B. Norton, B.A. Watkins, M.P. Buhr, D.D. Parrish, J.G. Calvert, and F.C. Fehsenfeld, An Intercomparison of 5 Ammonia Measurement Techniques, *Journal of Geophysical Research-Atmospheres*, *97* (D11), 11591-11611, 1992.

Yin, F.D., D. Grosjean, and J.H. Seinfeld, Photooxidation of Dimethyl Sulfide and Dimethyl Disulfide .1. Mechanism Development, *Journal of Atmospheric Chemistry*, *11* (4), 309-364, 1990.

Table 1. Species found to react with $(C_2H_5OH)_nH^+$ with ion molecule rate coefficients $> 2 \times 10^{-12}$ cm^3 $molec^{-1}$ s^{-1}

Species	P.A.	k_{Cal}	k_{Low}	k_{mid}	k_{High}
DMSO	211.4	2.2	1.8	1.5	0.35
NH_3	204	1.9	1.5	0.7	>.0025*
Acetone	194	1.9	1.0	nr	nr
MVK	199.5		1.6	nr	nr
$DMSO_2$	?		0.1 - 1.0	nr	nr

P.A. - proton affinity (kcal/mol) [*Hunter and Lias,*, 2000]
k_{Cal} - calculated collisional rate constant (10^{-9} cm^3 $molec^{-1}$ s^{-1}) [*Su and Chesnavich,* 1982]
k_{Low} - 24 ppbv ethanol/N_2 reagent mixture (10^{-9} cm^3 $molec^{-1}$ s^{-1})
k_{mid} - 900 ppmv ethanol/N_2 reagent mixture (10^{-9} cm^3 $molec^{-1}$ s^{-1})
k_{High} -1% ethanol/N_2 reagent mixture (10^{-9} cm^3 $molec^{-1}$ s^{-1})
nr - rate constant $< 2 \times 10^{-12}$ cm^3 $molec^{-1}$ s^{-1}
* - system equilibrates

Table 2. Species found to react with $(C_2H_5OH)_nH^+$ with ion molecule rate coefficients $< 2 \times 10^{-12}$ cm^3 $molec^{-1}$ s^{-1}

Species	P.A.	Species	P.A.	Species	P.A.
Methane	129.9	Trans-2-butene	179	2-pentanone	199.8
Acetylene	153.3	n-butane	?	Ethyl acetate	199.7
Ethylene	162.6	Isobutane	162	Cyclobutene	187.5
Ethane	142.5	Isopropanol	189.5	α-pinene	?
Methanol	180.3	Isobutylene	191.7	Ethyl Acetate	?
Propyne	179	Methylcyclohexane	?	1,3-butadiene	187.2
Propylene	179.6	Methacrolein	193.3	m-xylene	194.1
DMS	198.6	Cyclopentane	?	o-xylene	190.2
Isoprene	189.5	Methylcyclopentane	?	Ethylbenzene	188.3
Toluene	187.4	4-methyl-2-pentene	?	Methylbutenol	?
1-butene	?	3-methyl-2-pentene	194.3	Methyl Isobutyl Ketone	?
cis-2-butene	?	2-methyl-2-pentene	194		

P.A. - proton affinity (kcal/mol) [*Hunter and Lias*, 2000]

Figure Captions

Figure 1. Diagram of the ion-molecule reactor used in this study.

Figure 2. Panel A, mass spectrum taken in the boundary layer at 75 % relative humidity during PEM-Tropics B flight 16. Panel B, mass spectrum taken in the laboratory at 80 % relative humidity. (Note, the y-axis is linear from 0 - 1000 Hz and logarithmic above 1000 Hz.) Dominant peaks in both spectrum at high relative humidity are ethanol monomer and dimer. In panel B, the peak present at 61 amu is isopropanol impurity present in the ethanol used to generate the reagent ions.

Figure 3. DMSO time series plot for midday boundary and buffer layer sampling during PEM-Tropics B flight 16. DMSO observations are represented by (+) and the altitude by the solid line. Data are presented at a time resolution of 15 seconds.

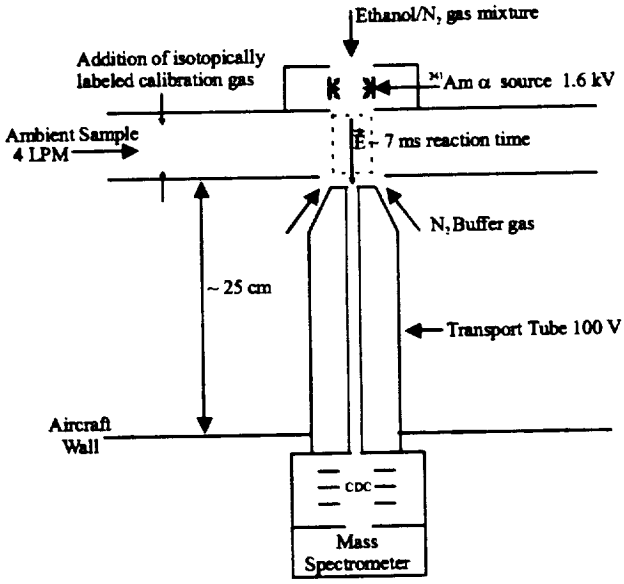
Ethanol/N, gas mixture
Addition of isotopically labeled calibration gas
^{241}Am α source 1.6 kV
Ambient Sample 4 LPM
~ 7 ms reaction time
N, Buffer gas
~ 25 cm
Transport Tube 100 V
Aircraft Wall
CDC
Mass Spectrometer

Figure 1

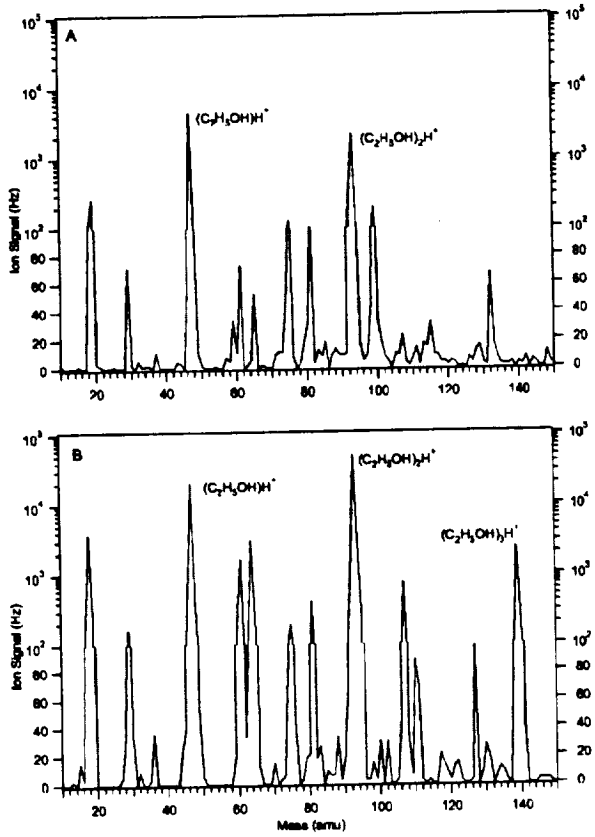

Figure 2

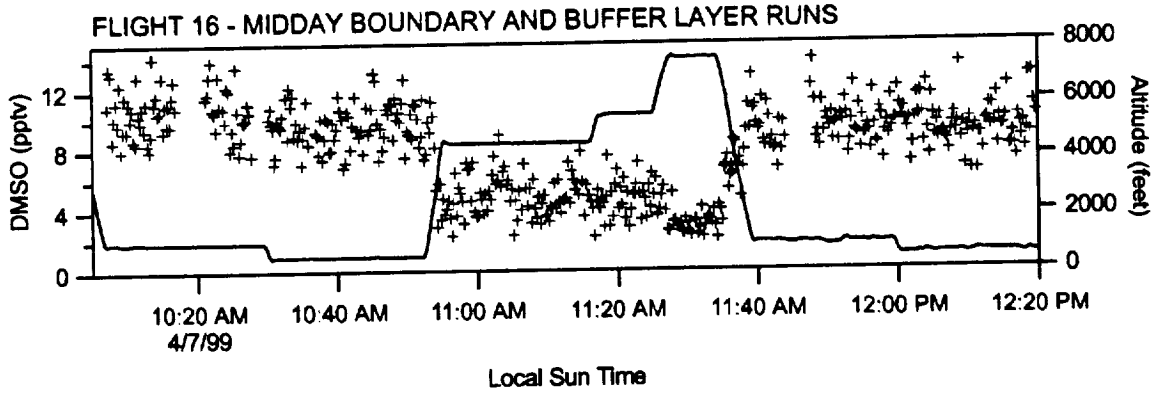

Figure 3

GEOPHYSICAL RESEARCH LETTERS, VOL. 28, NO. 11, PAGES 2201-2204, JUNE 1, 2001

Airborne Observations of DMSO, DMS, and OH at Marine Tropical Latitudes

J.B. Nowak[1], D. D. Davis[1], G. Chen[1], F. L. Eisele[1,2], R. L. Mauldin III[2], D. J. Tanner[2], C. Cantrell[2], E. Kosciuch[2], A. Bandy[3], D. Thornton[3], and A. Clarke[4]

Abstract – This paper reports the first simultaneous fast-time resolution measurements of dimethylsulfide (DMS), dimethylsulfoxide (DMSO), and the hydroxyl radical (OH) at marine tropical latitudes. These observations were recorded during the PEM-Tropics B field program on NASA's P-3B aircraft. The observations of DMSO, using a Selected Ion Chemical Ionization Mass Spectrometry (SICIMS) technique, are of particular significance. They have revealed two unique findings: 1) average midday-tropical levels of DMSO are significantly higher than those predicted from current models when constrained by observed DMS and OH levels (e.g., 10 pptv versus 1 to 3 pptv); and 2) DMSO concentration profiles are significantly out-of-phase with model predictions, maximum values being seen under near dark conditions and minimum values being observed at midday. Although no simple explanation has yet been found for these unusual results, the fact that no evidence points to a problem in the measurements suggests that others may exist. Clearly, if the observations are correct, they indicate that at least for tropical upwelling regions the atmospheric sulfur budget may need to be adjusted to accommodate additional sources of DMSO.

Introduction

Since the mid-1980s, dimethylsulfide (DMS) has been recognized as an important species in the scientific community's assessment of global climate change. This reflects the fact that the oxidation of ocean released DMS has been found to be an important marine source of sulfur dioxide (SO_2) in remote regions. Thus, it can ultimately lead to the formation of sulfate aerosol particles [e.g., *Charlson et al.*, 1987; *Berresheim et al.*, 1995 and references therein]. In past efforts to better quantify the details of the DMS oxidation process, laboratory as well as field studies have revealed that DMSO is a significant intermediate oxidation product (i.e., see Figure 1 and *Turnipseed et al.*, [1996]; *Davis et al.*, [1998]). In fact, current thinking is that the OH/DMS reaction is the dominant source of atmospheric DMSO.

Here we report the first simultaneous fast-time resolution measurements of DMSO and the closely coupled chemical species DMS and OH. These airborne measurements were recorded over the tropical Pacific Ocean during the NASA GTE PEM-Tropics B field program. Because of their time resolution, these observations have provided an excellent opportunity to explore the detailed chemistry controlling marine atmospheric levels of DMSO.

Experimental Techniques and Model Description

In the current study, DMSO measurements were made using a Selected Ion Chemical Ionization Mass Spectrometry (SICIMS) technique modified from that used by *Berresheim et al.* [1998]. Typically, 4 SLPM of ambient air is sampled through a ¾" Teflon inlet tube into the reaction region where DMSO was converted into $DMSOH^+$ by reaction with the reagent ion $(C_2H_5OH)_xH^+$. The $(C_2H_5OH)_xH^+$ ions were generated using a radioactive source and accelerated across the reaction region by electric fields. Product $DMSOH^+$ ions were then sampled with a quadrupole mass spectrometer and detected using an electron multiplier.

The SICIMS instrument was calibrated by the constant addition of a known amount of isotopically labeled C^{13} DMSO ($^{13}CH_3OS^{13}CH_3$) from a permeation tube. The permeation rate was determined gravimetrically by the manufacturer and is traceable to NIST standards. The tube was kept in a temperature controlled oven with constant N_2 flow maintained over it. The nitrogen/C^{13} DMSO mixture was diluted using a multi-stage dynamic dilution system before being added to the inlet where final dilution occurred with ambient air. The typical levels of C^{13} DMSO in the inlet were 100 pptv. Background measurements were performed by over filling the inlet with dry N_2 or zero air. A potential interference considered in this system was the formation of DMSO from ambient DMS. Further laboratory testing under simulated marine conditions, however, showed no artifact DMSO production and no interference at the C^{13} $DMSOH^+$ calibration mass. The combined uncertainty of the permeation tube and dilution system is estimated at ± 50% and primarily reflects the uncertainty associated with the emission rate of the DMSO permeation tube. The detection limits for 1 and 10 minute integration times were estimated to be 1 and 0.3 pptv, respectively, for a signal to noise ratio of 2 to 1. (A more detailed description of the DMSO SICIMS system is provided by J.B. Nowak et al., *Chemical Ionization Mass Spectrometry Technique for the Detection of Dimethylsulfoxide and Ammonia*, submitted 2001)

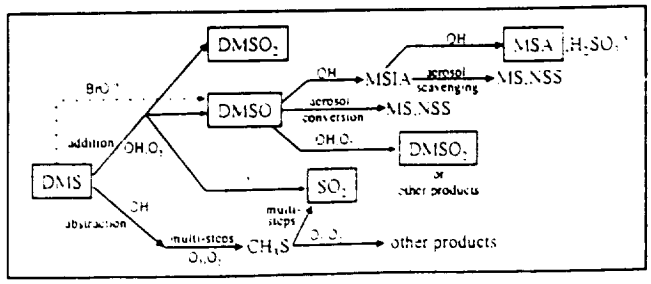

Figure 1. Abbreviated DMS/OH atmospheric oxidation scheme.

[1]School of Earth and Atmospheric Sciences, Georgia Institute of Technology, Atlanta, GA, 30332, USA.

[2]Atmospheric Chemistry Division, National Center for Atmospheric Research, Boulder, CO, 80303, USA.

[3]Dept. of Chemistry, Drexel U., Philadelphia, PA, 19104, USA.

[4]Dept of Oceanography, University of Hawaii, Honolulu, HI, 96822, USA.

Paper number 2000GL012297.
0094-8276/01/2000GL012297$05.00

Table 1. PEM Topics B DMS and DMSO Observations

		DMSO		DMS	
		Mean (pptv)	Range (pptv)	Mean (pptv)	Range (pptv)
BL	Flt 15	4.5	2.3 - 8.9	130	66 - 185
	Flt 16	11.5	7.2 - 17.9	269	179 - 358
	Flt 17	5.3	2.9 - 9.4	135	114 - 150
		Mean (pptv)	Range (pptv)	Mean (pptv)	Range (pptv)
BuL	Flt 15	3.6	<1.0 - 6.3	82	61 - 96
	Flt 16	5.4	4.2 - 7.6	108	63 - 191
	Flt 17	3.7	<1.0 - 7.1	75	68 - 85

Flt 15: 16°S/148°W, Flt 16: 13°S/143°W, Flt 17: 2°N/154°W

Measurements of DMS were made using gas-chromatography mass-spectrometry with cryogenic trapping previously described by *Bandy et al.* [1993]. The data collection rate for the PEM-Tropics B system was typically one sample every 5 min with a limit of detection (LOD) of 2 pptv. The uncertainty was ±10% when DMS was at levels greater than five times the LOD. Measurements of OH were made using a SICIMS technique previously described by *Mauldin et al.* [1999]. The nominal time resolution for this system was 10 s although data were typically blocked as 1 to 5 min averages resulting in an LOD for this species in the range of $1 - 2 \times 10^5$ molec/cm^3. The uncertainty in these measurements when the signal was five times greater than the LOD is estimated at ± 40% (2σ).

The model simulations reported here are based on a sulfur box model that contained 14 sulfur reactions describing both the sources and sinks of DMS, sulfur dioxide (SO_2), sulfuric acid (H_2SO_4), methane sulfonic acid (MSA), DMSO, dimethylsulfone ($DMSO_2$), methane sulfonate (MS), methane sulfinic acid (MSIA), and non-sea-salt sulfate (NSS) [*Davis et al.*, 1998, 1999]. It has been used in this study to simulate the diel profiles of DMSO, SO_2, and H_2SO_4. A critical parameter assumed in the current sulfur model is the conversion efficiency of DMS to DMSO. For the abstraction branch this efficiency was taken to be zero. For the addition channel, which is only 25% of the total, values from 0.5 to 1.0 were used. This range reflects both the most recent analysis of sulfur field data by *Davis et al.* [1998, 1999] as well as DMS laboratory gas kinetic studies [*Turnipseed et al.*, 1996; *Hynes et al.*, 1993; *Arsene et al.*, 1999]. In the current investigation, DMSO simulations were constrained by DMS and OH observations as well as by the total aerosol surface area. The latter was evaluated using data from a differential mobility analyzer (0.02< Dp <0.5μm) and an optical particle counter (0.148 <Dp <6μm).

For time periods when OH data were not available, the OH profile was generated from a coupled photochemical time-dependent box model, previously described by *Crawford et al.* [1999]. This model includes full $HO_x/NO_x/CH_4$/NMHC chemistry. Input consists of measured values for NO, CO, H_2O, O_3, UV irradiance, and nonmethane hydrocarbons (NMHC's) as well as for meteorological parameters [*Raper et al.*, 2000].

Observations and Discussion

DMSO was measured on flights 15, 16, and 17 during PEM-Tropics B. Table 1 presents a summary of both the DMSO and DMS data from these flights. Information is provided for both the boundary layer (BL) and the overlying transition zone between the BL and free troposphere (labeled here the buffer layer (BuL) as defined by *Russell et al.* [1998]). Of the BL DMSO observations shown, those recorded during flight 16 were the most comprehensive in that covered the largest fraction of the solar window. They also encompass the highest values recorded. All flight 16 BL observations were recorded at/or below 300m; whereas, most of the BuL measurements were made at 1500m.

As discussed in the text below, flight 16 was the only flight that was downwind of the Marquesas Islands. Although the observations from flight 15 were geographically further downwind from those recorded on flight 16, they were made near sunset. Thus, they were some of the lowest values observed during the three flights in which DMSO was measured. Flight 17 was a transit flight from Tahiti to Hawaii and the BL/BuL data reported were those recorded near Christmas Island at 2.5°N around solar high noon. Earlier flights in this region revealed that, on average, this location had lower midday DMS values than those recorded during flight 16.

The marine region sampled during flight 16 has been shown to be strongly influenced by an island mass-effect due to the presence of the Marquesas Islands to the east [*Signorini et al.*, 1999]. As a result, large enhancements in surface chlorophyll and DMS (previously reported by *Yvon et al.* [1996]) are typically found as the Southern Equatorial Current flows around the islands. The net effect of the latter is that overhead atmospheric levels of DMS typically have been found to reach several hundred pptv [e.g., *Yvon et al.*, 1996].

Because of its uniqueness in providing DMS and DMSO levels as a function of solar intensity, the remainder of this text primarily focuses on the analysis of the flight 16 data. As shown in Figure 2a, BL data was recorded during flight 16 from approximately 0700 to 1330 on 7 April 1999, covering a significant fraction of the solar window. The sampling pattern executed during flight 16 followed an Eulerian scheme in which

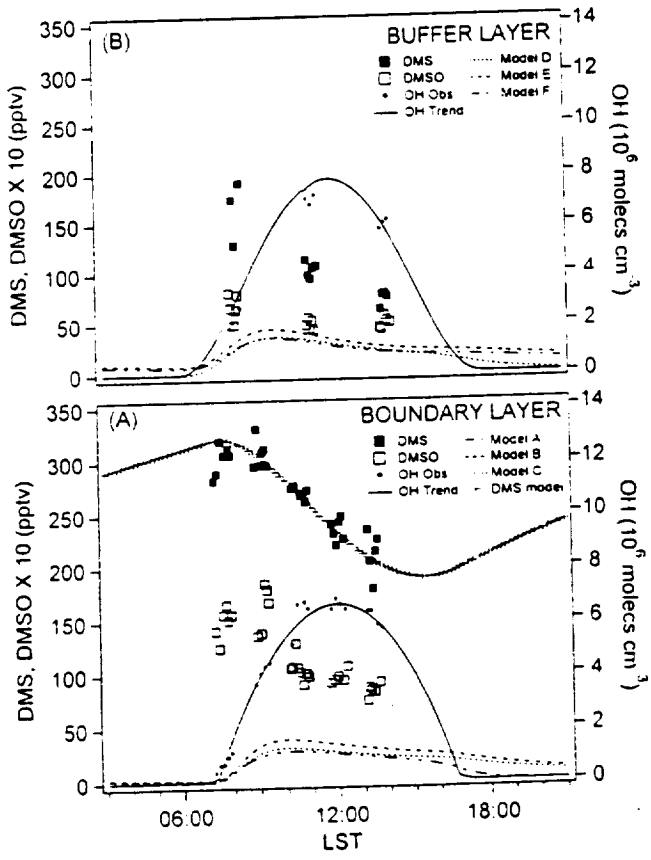

Figure 2. Diurnal trends of DMS and DMSO during flight 16: BL (bottom panel), BuL (top panel). All observational data have been averaged to 10 min intervals. The 1σ deviation for a 10 min DMSO average was ± 16% for the BL and ± 25% for the BuL. The 1σ deviation in the OH data was estimated at ± 19% for the BL and ± 12% for the BuL. Similar estimates for DMS gave a 1σ deviation of ± 6% for the BL and ± 12% for the BuL. The branching ratio and the overall lifetime for DMSO for each model simulation are given in Table 2.

Table 2. Summary of DMSO Model Simulations

Model Run	Branching Ratio	DMSO Aerosol Lifetime[1]	DMSO Overall Lifetime[2]
A	1.0	1 hr	0.8 hrs
B	1.0	6 hrs	2.4 hrs
C	0.8	6 hrs	2.4 hrs
D	1.0	2 hrs	1.2 hrs
E	1.0	13.5 hrs	2.7 hrs
F	0.8	13.5 hrs	2.7 hrs

[1] Lifetime with respect to aerosol scavenging

[2] Lifetime with respect to aerosol scavenging and photochemical oxidation

four designated altitudes were sampled multiple times but at approximately the same geographical coordinates (e.g., 13°S and 143°W). The aircraft's horizontal racetrack shaped flight legs were flown orthogonal to the wind field and the corresponding fetch for this wind regime was well over 800 km.

As seen in Figure 2, two unique aspects of flight 16 are: 1) levels of DMSO are quite high (e.g., BL, 7-18 pptv), and 2) the trend in DMSO does not follow what one might predict based on the DMS/OH reaction being the major source of DMSO. The highest observed levels are found at/or near dark conditions (sunrise); while, the lowest values are recorded around high noon. The BL DMSO trend also parallels that observed for DMS. As shown in figure 2a, the model simulated DMS profile, as constrained by a model estimated DMS flux and observed OH, closely tracks the experimentally observed DMS profile. This agreement argues strongly against the possibility that the DMS and DMSO profiles were somehow controlled by abrupt shifts in the sampled air mass during flight 16.

The three model profiles presented in Figure 2a, are all based on the assumption that the DMS/OH reaction is the sole source of DMSO. They suggest that the maximum value of DMSO should occur around 1000 LST. Model A assumes a conversion efficiency for DMS to DMSO of 1.0 (e.g., *Arsene et al.* [1999]). It also assumes that aerosol scavenging of DMSO is primarily controlled by its sticking coefficient (i.e, irreversible) as reported by *De Bruyn et al.* [1994]. Model B, uses the same DMS to DMSO conversion yield, but the scavenging efficiency of DMSO is limited by the rate of aqueous phase chemistry that forms MS from DMSO. In model C, it is assumed that the DMS to DMSO conversion efficiency is closer to that estimated from field studies (e.g., 0.8) as reported in the analysis by *Davis et al.* [1998] and that the scavenging rate is the same as used in model B. Given this range of values for critical DMSO parameters, the scavenging lifetime was estimated to be 1 hr for model A and 6 hrs for both models B and C. However, upon folding in the loss of DMSO due to photochemistry, the overall DMSO lifetime is found to drop to 0.8 hrs for model A and 2.4 hrs for both models B and C (e.g., see Table 2). The authors note that if the assumption is made that the conversion efficiency for DMS to DMSO is closer to 0.5 (as per the laboratory kinetic results of *Turnipseed et al.* [1996] and *Hynes et al.* [1993]), predicted DMSO levels still drop another 20-30%.

Shown in Figure 2b are the flight 16 DMSO data recorded in the BuL. Again, a similar diurnal trend in DMSO is seen as that shown in Figure 2a. The major difference between the BL and BuL DMSO profiles appears in the average mixing ratio values. For the BuL the range is 4 to 8 pptv, with an average of 5.4 pptv; whereas, for the BL it is 7 to 18 pptv with an average of 11.5 pptv.

The DMSO model simulations for the BuL are also shown in Figure 2b as model runs D, E, and F. The general assumptions stated for model runs A, B, and C, apply to the equivalent BuL runs D, E, and F. However, because of the lower aerosol loading of the BuL, the estimated DMSO lifetime has been increased. For model run D, it was 2 hrs; and for both model runs E and F it was 13.5 hrs. Folding in photochemical loss, the overall lifetimes for the above cases were 1.2 and 2.7 hrs (see Table 2). If the most favorable set of assumptions is made in the BuL simulations, the model predicted value of DMSO can be moved to within a factor of 2 of the observations. This difference is within the combined uncertainties of the measurements and model calculations. On the other hand, for the BL case, the difference between observations and the most favorable model profile is still a factor of 3 lower at midday and over an order of magnitude lower for early morning hours. The largest uncertainty in this simulation is in the DMSO aerosol scavenging rate. However, even assuming no aerosol scavenging/dry deposition loss, the model simulated DMSO profile is still lower than the observations for early morning hours by a factor of 6.

The magnitude of the difference separating the model predictions and observations would initially suggest that either the measurements are in error or that there are problems with the model. Concerning possible modeling shortfalls, the most obvious of these is that there are other DMSO sources. In addition, there is the issue of vertical transport. The fact that the BuL had nearly half as much DMS as the BL is a strong indication that convection was quite significant in the 24 hours preceding flight 16. Both real time photographical records and a detailed meteorological analysis of the region using satellite imagery have confirmed this. Thus, it stands to reason that the same convective processes that were responsible for transporting significant amounts of DMS from the BL to the BuL also were responsible for transporting a significant fraction of BL DMSO into the BuL. The most effective time period for this would have been under dark conditions. Given this scenario, a DMS model simulation was carried out in which parameterized transport was included. The resulting DMS mixing parameter was then employed for assessing the impact of transported DMSO on the BuL. Although this addition increased the BuL DMSO by another 40%, it leaves the BL DMSO discrepancy just as large as it was in the beginning.

Returning to the possibility that other DMSO sources might exist in addition to the DMS/OH reaction, the tropical DMSO data reported by *Bandy et al.* [1996] prove interesting. These are the only other tropical data having a time resolution of less than an hour. Quite significant here were the findings that DMSO levels were also highly elevated (e.g., 10-50 pptv). Also, when all data were plotted on a common 24 hr time axis, the diurnal trend showed the highest values to be under dark conditions, decreasing toward mid-day. Using the same sulfur model, simulations based on measured DMS were found to under-predict the observed DMSO by factors of 25 to 50, depending on the assumptions made concerning the DMS-to-DMSO conversion efficiency and the aerosol loss rate for DMSO [*Chen et al.*, 2000]. Collectively, both tropical DMSO data sets would seem to point toward an alternative tropical DMSO source.

Here we speculate on two other DMSO sources in the tropical marine troposphere. The first of these involves the halogen reaction, BrO + DMS. Previously, *Toumi* [1994] estimated that as much as 10% of the global oxidation of DMS could occur via the reaction with BrO. More recently, *Ingham et al.* [1999] have reported a rate coefficient for this reaction that would double this prediction. In spite of these favorable kinetic developments, there remains two serious problems with this hypothesis. First, a significant tropical marine source of BrO has yet to be observed; and second, model simulations reveal that at night BrO would be rapidly depleted by its reaction with formaldehyde (CH_2O). Since, in the tropics, significant levels of CH_2O persist through the night, the latter shortcoming would seemingly make it impossible to account for the observed dark or near dark DMSO observations that have been reported by *Bandy et al.* [1996] and in the current study.

The second possibility might involve release of DMSO from the ocean itself. Recognizing that a similar diurnal trend is found

between DMS and DMSO in both the Bandy data and during flight 16, it is tempting to speculate that these two species may have a common source. This possibility becomes even more intriguing when it is recognized that marine observations have shown that DMSO can be 10 to 20 times higher in concentration in the water column than DMS [*Lee et al.*, 1999 and references therein]. On the other hand, since DMSO is far more soluble than DMS (e.g., Henry's Law constant 1.17×10^5 versus 0.49 mol kg^{-1} atm^{-1} [*Watts and Brimblecombe*, 1987; *Sander*, 2000]), it is difficult to see how this mechanism might explain the high levels of DMSO in the BL.

Revisiting the possibility that major errors might exist in the observations themselves has turned up no leads. Critical here have been the laboratory tests which have shown no evidence of a DMS to DMSO conversion within the ion-molecule reactor. Although quite limited in number, other non-tropical DMSO observations do not appear to show the same trends observed in the tropics [e.g., *Davis et al.*, 1998; *Sciare et al.*, 2000]. Both the presence of upwelling and deep convection at the tropical latitudes of this study may be important factors, but at this time we have not been able to show a simple causal relationship. Clearly, additional BL tropical field observations of DMSO, DMS, and OH together with water column measurements of DMSO are needed. If there is indeed an additional source of DMSO in the tropics, the natural global sulfur budget may need to be reexamined.

Acknowledgments - The author D. Davis would like to acknowledge the partial support of this research by NASA grant NCC-1-306. The author J.B. Nowak also acknowledges support from NASA Earth System Science Fellowship program. Finally, we would like to thank Drs. L. Gregory Huey, Paul Wine, and Ira Leifer for many insightful discussions.

References:

Arsene, C. I. Barnes, and K.H. Becker, FT-IR product study of the photooxidation of dimethyl sulphide: Temperature and O_2 partial pressure dependence, *Phys. Chem. Chem. Phys.*, *1*, 5463-5470, 1999.

Bandy, A. R., D. C. Thornton, A. R. Driedger III, Airborne measurements of sulfur dioxide, dimethyl sulfide, carbon disulfide, and carbonyl sulfide by isotope dilution gas chromatography/mass spectrometry, *J. Geophys. Res.*, *98*, 23,423-23,433, 1993.

Bandy A.R., D.C. Thornton, B.W. Bloomquist, S. Chen, T.P. Wade, J.C. Ianni, G.M. Mitchell, and W. Nadler, Chemistry of dimethyl sulfide in the equatorial pacific atmosphere, *Geophys. Res. Lett.*, *23*, 741-744, 1996.

Berresheim, H. P.H. Wine, and D.D. Davis, Sulfur in the atmosphere, in *Composition, Chemistry, and Climate of the Atmosphere*, edited by H.B. Sing, Van Nostrand Reinhold, New York, 1995.

Berresheim, H., J.W. Huey, R.P. Thorn, F.L. Eisele, D.J. Tanner, and A. Jefferson, Measurements of dimethyl sulfide, dimethyl sulfoxide, dimethyl sulfone, and aerosol ions at Palmer Station, Antarctica, *J. Geophys. Res.*, *103*, 1629-1637, 1998.

Charlson, R.J., J.E. Lovelock, M. O. Andreae, and S. G. Warren, Oceanic phytoplankton, atmospheric sulphur, cloud albedo and climate, *Nature*, *326*, 655-661, 1987.

Chen, G., D.D. Davis, P. Kasibhatla, A.R. Bandy, D.C. Thronton, B.J. Huebert, A.D. Clarke, and B.W. Bloomquist, A Study of DMS Oxidation in he Tropics: Comparison of Christmas Island Field Observations of DMS, SO_2, and DMSO with Model Simulations, *J. Atm. Chem.*, *37*, 137-160, 2000.

Crawford, J. H., D. D. Davis, J. Olson, G. Chen, S. Liu, S. Sandhoim, B. Heikes, G. Gregory, D. Blake, and H. Singh, An assessment of upper tropospheric HOx sources over the tropical Pacific based on NASA GTE PEM data: net effect on HOx and other photochemical parameters, *J. Geophys. Res.*, *104*, 16,255-16273, 1999.

Davis, D. D., G. Chen, P. Kasibhatla, A. Jefferson, D. Tanner, F. Eisele, D. Lenschow, W. Neff, and H. Berresheim, DMS oxidation in the Antarctic marine boundary layer I: Comparison of model simulations with field observations for DMS, DMSO, $DMSO_2$, H_2SO_4(g), MSA(g), and MSA(p), *J. Geophys. Res.*, *103*, 1657-1678, 1998.

Davis, D. D., et al., Dimethyl sulfide oxidation in the equatorial Pacific: Comparison of model simulations with field observations for DMS, SO_2, H_2SO_4(g), MSA(g), MS, and NSS, *J. Geophys. Res.*, *104*, D5, 5,765-5,784, 1999.

DeBruyn, W. J., J. A. Shorter, P. Davidovits, D. R. Worsnop, M. S. Zahniser, and C. E. Kolb, Uptake of gas phase sulfur species methanesulfonic acid, dimethylsulfoxide, and dimethyl sulfone by aqueous surfaces, *J. Geophys. Res.*, *99*, 16,927-16,932, 1994.

Hynes, A.J., R.E. Stickel, A.J. Pounds, Z. Zhao, T. Mckay, J.D. Bradshaw, and P.H. Wine, Mechanistic studies of OH-initiated oxidation of dimethylsufide, in *Dimethylsulfide: Oceans, Atmospheres, and Climate*, edited by G. Restelli and G. Angeletti, p. 211, Kluwer Academic, Newell, Mass., 1993.

Ingham, T., D. Bauer, R. Sander, P.J. Crutzen, and J.N. Crowley, Kinetics and products of the reactions BrO + DMS and Br + DMS at 298 K, *J. Phys. Chem. A*, *103*, 7199-7209, 1999.

Lee, P.A., S.J. de Mora, and M. Levasseur, A review of dimethylsulfoxide in aquatic environments, *Atmosphere-Ocean*, *37*, 439-456, 1999.

Mauldin III, R. L., D. J. Tanner, and F. L. Eisele, Measurements of OH during PEM-Tropics A, *J. Geophys. Res.*, *104*, 5817-5827, 1999.

Raper, J.L., M.M. Kleb, D.J. Jacob, D.D. Davis, R.E. Newell, H.E. Fuelberg, R.J. Bendura, J.M. Hoell, and R.J. McNeal, Pacific Exploratory Mission in the Tropical Pacific: PEM-Tropics B, March-April 1999, *J. Geophys. Res.*, accepted, 2001.

Russell, L.M, Lenschow, D.H., Laursen, K.K., Krummel, P.B., Siems, S.T., Bandy, A.R., Thornton, D.C., and Bates, T.S., Bidirectional mixing in an ACE 1 marine boundary layer overlain by a second turbulent layer, *J. Geophys. Res.*, *103*, 13, 16,411-16,432, 1998.

Sander, R. "Henry's Law Constants" in NIST Chemistry WebBook, NIST Standard Reference Database Number 69, Eds. W.G. Mallard and P.J. Linstrom, February 2000, National Institute of Standards and Technology, Gaithersburg MD, 20899 (http://webbook.nist.gov).

Sciare, J. M. Kanakidou, and N. Mihalopoulous, Diurnal and seasonal variation of atmospheric dimethylsulfoxide at Amsterdam Island in the southern Indian Ocean, *J. Geophys. Res.*, *105*, 17,25-17,265, 2000.

Signorini, S.R., C.R. McClain, and Y. Dandonneau, Mixing and phytoplankton bloom in the wake of the Marquesas Islands, *Geophys. Res. Lett.*, *26*, 3121-3124, 1999.

Toumi, R., BrO as a sink for dimethylsulphide in the marine atmosphere, *Geophys. Res. Lett.*, *21*, 117-120, 1994.

Turnipseed, A. A., S. B. Barone, and A. R. Ravishankara, Reactions of OH with DMS. II. Products and Mechanisms, *J. Phys. Chem.*, *100*, 14,703-14,713, 1996.

Watts, S.F. and P. Brimblecombe, The Henry's Law constant of dimethyl sulphoxide, *Environ. Technol. Lett.*, *8*, 483-486, 1987.

Yvon, S.A., E.S. Saltzman, D. J. Cooper, T.S. Bates, and A.M. Thompson, Atmospheric sulfur cycling in the tropical Pacific marine boundary layer (12°S, 135°W): A comparison of field data and model results 1. Dimethylsulfide, *J. Geophys. Res.*, *101*, 6899-6909, 1996.

G. Chen, D.D. Davis, F.L. Eisele, and J.B. Nowak, School of Earth and Atmospheric Sciences, Georgia Tech, 221 Bobby Dodd Way, Atlanta, GA 30332-0340. (email: dd16@prism.gatech.edu)

C.Cantrell, F.L. Eisele, E. Kosciuch, R.L. Mauldin III, and D.J. Tanner, ACD, NCAR, P.O. Box 3000, Boulder, CO, 80303-3000.

A.R. Bandy and D.C. Thornton, Dept. of Chemistry, Drexel University, 3141 Chestnut St. Philadelphia, PA 19104.

A. Clarke, Dept. of Oceanography, University of Hawaii, 1000 Pope Rd., Honolulu, HI, 96822.

(Received September 5,2000; revised February 20,2001; accepted February, 20, 2001.)